Universidade de Aveiro Departamento de Electrónica e Telecomunicações
2009

Hélder Pedro Lopes Moura

Análise de redes de rádio sobre fibra óptica

Dissertação apresentada à Universidade de Aveiro para cumprimento dos requisitos necessários à obtenção do grau de Mestre em Engenharia Electrónica e Telecomunicações, realizada sob a orientação científica do Dr. Paulo Miguel Nepomuceno Pereira Monteiro, Professor Doutor do Departamento de Electrónica e Telecomunicações da Universidade de Aveiro.

Dedico este trabalho, indubitavelmente, aos meus pais e irmãs.

o júri

presidente

Prof. Dr. António Luís Jesus Teixeira
professor associado do Departamento de Electrónica, Telecomunicações e Informática da Universidade de Aveiro

Prof. Dr. Paulo Miguel Nepomuceno Pereira Monteiro
professor associado do Departamento de Electrónica, Telecomunicações e Informática da Universidade de Aveiro

Prof. Dr. Rui Fernando Gomes de Sousa Ribeiro
professor auxiliar do Departamento de Electrónica, Telecomunicações e Informática da Universidade de Aveiro

Prof. Dr. Henrique Manuel de Castro Faria Salgado
professor associado da Faculdade de Engenharia da Universidade do Porto

agradecimentos

No decorrer deste trabalho, existiram várias pessoas a quem, de alguma forma, penso necessário demonstrar o meu agradecimento. Não sendo possível apontar todos os nomes em questão, apenas destaco aqueles que foram mais preponderantes.

Para começar, gostaria de agradecer ao meu orientador, prof. Paulo P. Monteiro que sempre me disponibilizou toda a ajuda que foi necessária no decorrer do trabalho de dissertação. Ao meu co-orientador, prof. Rui S. Ribeiro, tenho a agradecer a intensiva dedicação com que sempre me acompanhou e cujas análises científicas foram fulcrais para o desenvolvimento deste trabalho assim como para o meu enriquecimento profissional.

Agradeço aos meus pais, João e Dília, e irmãs, Dina e Cátia, por todo o apoio e confiança que sempre depositaram em mim. Ao meu avô, Manuel Morrão.

Durante o meu percurso académico, foi indiscutível a importância dos meus amigos, tanto da Universidade de Aveiro como os da minha terra natal, Granja, que sempre me incluíram no seu círculo. Gostava de salientar o Victor, da Granja e, da universidade, o meu grande amigo João Lima, que ao longo do curso sempre dispôs da sua amizade e conhecimento para me ajudar. Além destes, nomes como Soares, Henriques, Nuno e Maia, da universidade de Aveiro, e Pedro Gerardo e José Manuel, da Granja, merecem destaque.

Gostava de agradecer à Liliana, uma amiga.

Hélder Moura

palavras-chave Radio sobre Fibra, WLAN, Modulação Externa, Modulação Directa

resumo

Este trabalho teve como objectivo a implementação e simulação de dois sistemas óptico-analógicos possíveis para a transmissão de sinais rádio sobre fibra óptica. O primeiro utilizando modulação externa, e o segundo modulação directa.

Foram implementados modelos necessários para a modelação/transmissão de sinais rádio, bem como a sua desmodulação/recepção. Estes modelos foram adaptados ao software de simulação óptica OSIP, de modo a permitir a simulação de Rádio sobre Fibra. Para validar os resultados, foram utilizados valores obtidos de simulações com o software VPI©, assim como medidas experimentais.

keywords Radio over Fiber, WLAN, External Modulation, Direct Modulation

abstract

The objective of the presented work was to implement and simulate two different analog optical systems for the transmission of radio signals over optical fiber. The first one with external modulation, and the second with direct modulation.

In order to make this possible, were implemented necessary models to the modulation/transmission of radio signals, as well as the respective demodulator/receiver. Those models were adapted to the optical simulation software OSIP, to allow the Radio over Fiber simulation. To validate the results were used experimental measurements, as well as results from VPI©, another simulation software.

Table of Contents

List of Acronyms

APD	Avalanche photodetector
BB	*Baseband*
BPF	*Bandpass Filter*
BS	*Base Station*
B-ISDN	*Broadband Integrated Services Digital Network*
CMOS	*Complementary metal–oxide–semiconductor*
CNR	*Carrier to Noise Ratio*
CO	*Central Office*
CW	*Continuous Wave*
DFB	*Distributed Feedback*
DWDM	*Dense Wavelength Division Multiplex*
EMI	*Electromagnetic Interference*
EVM	*Error Vector Magnitude*
GVD	*Group Velocity Dispersion*
IEEE	*Institute of Electrical and Electronics Engineers*
IF	*Intermediate Frequencies*
IMD	*Intermodulation Distortion*
IM2	*Second-order Intermodulation Distortion*
IM3	*Third-order Intermodulation Distortion*
IM-DD	*Intensity Modulation – Direct Detection*
IT	*Instituto de Telecomunicações*
ISM	*Industrial, Scientific and Medical*
ITS	*Intelligent Transport System*
IVC	*Inter-Vehicle Communication*
MBS	*Mobile Broadband System or Service*
MIMO	*Multiple-Input Multiple-Output*
MMF	*Multimode Fiber*
MU	*Mobile Unit*
MVDS	*Multi-point Video Distribution Services*
MZM	*Mach-Zehnder Modulator*

M-QAM	*Mary Quadrature Amplitude Modulation*NF *Noise Figure*
OFDM	*Orthogonal Frequency Division Multiplex*
RAU	*Remote Antenna Unit*
RF	*Radiofrequency*
RIN	*Relative Intensity Noise*
RoF	*Radio-over-Fiber*
RVC	*Road-to-Vehicle Communication*
SCM	*Subcarrier Modulation*
SEONs	*Symposium of Enabling Optical Networks and Sensors*
SFDR	*Spurious Free Dynamic Range*
SMF	*Single Mode Fiber*
UMTS	*Universal Mobile Telecommunications System*
UWB	*Ultra Wideband*
WDM	*Wavelength Division Multiplex*
WiMAX	*Worldwide Interoperability for Microwave Access*
WLAN	*Wireless Local Area Network*
VSCEL	*Vertical-Cavity Surface-Emitting Laser*

List of Symbols

P_0	Optical power at the beginning of the fiber
P_L	Optical power at the output of a L km length liber
α	Attenuation coefficient
α_R	Rayleigh attenuation coefficient
C_R	Rayleigh coefficient
λ	Wavelength
D_m	Material Dispersion
c	Light velocity in vacuum
n_1	Refractive index of the core
n_2	Refractive index of the cladding
Δ	Fractional index change
a	Core Radius
D_w	Waveguide dispersion
R_m	Reflectivity of laser cleaved facets
I_{th}	Threshold current
n_l	Lasing medium refractive index
g_{th}	Lasing-threshold optical gain
α_i	Intrinsic losses
α_{mirror}	Mirror losses
L_c	Cavity length
m	Laser longitudinal modes
f	Frequency
Δf	Frequency variation
$\Delta\lambda$	Wavelength variation
σ	Gain spectrum width
$\overline{n}$	Average mode index

Λ	Grating period
m_B	Diffraction order
$S_p(t)$	Photon population
$N_p(t)$	Carrier population
$\phi(t)$	Optical field phase
$I(t)$	Injection current
τ_p	Photon lifetime
τ_n	Carrier lifetime
β_s	Spontaneous emission factor
N_{pt}	Transparency value of the carrier population
α_H	Linewidth enhancement factor
q	Electron charge
$f_s(t)$	Photon Langevin noise source
$f_n(t)$	Carrier Langevin noise source
$f_\phi(t)$	Phase Langevin noise source
$g_p(t)$	Stimulated emission gain for populations
ε	Nonlinear gain
ε_p	Normalized nonlinear gain
g_o	Differential gain
g_{po}	Normalized differential gain
Γ	Confinement factor
V_a	Active layer volume
g_m	Linear material gain coefficient
v_g	Group velocity
$N(t)$	Carrier density
$S(t)$	Photon density
S_{po}	Mean value of carrier population

N_{po}	Mean value of photon population
Q_n	Stimulated emission derivative relatively to carrier population
Q_p	Stimulated emission derivative relatively to photon population
γ_n	Decay rate of the small-signal carrier population
γ_p	Decay rate of the small-signal photon population
$H_A(\omega)$	Amplitude response
$H_F(\omega)$	Frequency response
η	Quantum efficiency
h	Planck constant
v	Optical frequency
I_o	Input mean current
w_{rr}	Relative frequency
$E(t)$	Optical field
$E_{CW}(t)$	Continuous wave optical field
$E_{lpCW}(t)$	lowpass equivalent of the continuous wave optical field
$I_{pin}(t)$	Photocurrent
$i_{pin}(t)$	Photocurrent small-signal term
P_{pin}	Incident *p-i-n* optical power
R	Photodetector Responsivity
$\theta_{MZM}(t)$	Optical phase shift through MZM arm
θ_0	Optical phase shift change related to the electro-optical material
V_π	MZM switching voltage
$E(t)$	Optical Field
A_{tt}	MZM insertion losses
$E_{MZM\_in}(t)$	Input MZM optical field
$E_{MZM\_out}(t)$	Output MZM optical field
$v(t)$	Time-varying voltage applied to MZM electrode

$v_{bp}(t)$	Bandpass time-varying voltage signal
$A(t)$	Time-varying signal amplitude
$\theta_e(t)$	Electrical phase shift
$\varphi_1(t)$	Inphase QAM carrier
$\varphi_2(t)$	Quadrature QAM carrier
T	Symbol period
s_k	*k*-th symbol of the QAM constellation
$d_{\min}$	Minimum distance between two neighbor points in the constellation
E_0	Energy of the lowest amplitude symbols
E_{av}	Average constellation energy
P_{av}	Average constellation power
a_k	Inphase amplitude of the *k*-th symbol
b_k	Quadrature amplitude of the *k*-th symbol
$v_{RF}(t)$	N symbols length signal
BW	QAM signal bandwidth
P_{s_k}	*k*-th symbol average power
$\bar{P}$	Signal mean power
S_x	Correction factor in power estimation
I_j	Received inphase symbol coordinate
Q_j	Received quadrature symbol coordinate
$\bar{I}_j$	Ideal inphase symbol coordinate
$\bar{Q}_j$	Ideal quadrature symbol coordinate
$\lvert v_{\max} \rvert$	Outermost ideal symbol magnitude of the QAM constellation
G_{em}	Externally modulated link gain
G_{dm}	Directly modulated link gain

1

Introduction

1.1 Motivation

In the last years, the implementation of optical fiber in the access networks to provide high bandwidth to the users and to be able to support the emerging and future services, is been taking place in Asia and America, and even in Europe it starts to be meaningful.

Nowadays, these optical networks are mainly used for transmission of data, video and voice fixed services. However, these can also be used (in simultaneous) to incorporate mobile traffic applications (Data and Voice) and wireless access (e.g. WLAN) leading to an optimization /minimization of the infrastructure costs. In this context and since wireless services use analog radio signals, the utilization of the RoF will be preponderant in the future access optical networks settlement. Furthermore, the wireless networks providers are

faced to supply more and more capacity to meet the constantly increasing requirements of the users. One way to overtake this problem is to increase the number of antennas to cover a certain cell, and the optical fiber shows to be the better way to connect them.

The simulating software most used nowadays in RoF systems is the VPI©, since it is the best known and with larger reliability. The recent development of OSIP within IT (*Instituto de Telecomunicações*), which runs over Matlab©, opens new opportunities in optical simulating systems, mainly from the fact that it is open source. However, it does not support RoF systems.

This work is framed in the FUTON project.

1.2 Objectives

Since OSIP does not have the models required to generate radiofrequency signals, it is an scope in this work to model the electrical signal generator initially for the 802.11g standard, as well as the receiver. To analyze the system performance, one has to model the EVM evaluator.

Another major objective is the modeling of a DFB laser in order to accept radiofrequency signals, to simulate the direct modulation scenario in RoF system.

The global objective of this work is finally to apply the implemented models in OSIP software, to both external and direct modulation scenarios for 802.11g standard in a RoF system.

1.3 Structure

This text is structured in 5 chapters which present the work done, from the acknowledgment of the technologies to the results obtained with the practical implementations.

In this first chapter, it is introduced the motivation to the work, as well as the scope, the structure of the dissertation and, the main contributions of the work developed.

The second chapter introduces several basic notions in the optical and electrical fields, required to fully understand the RoF concept, and its major advantages. In optics, are presented some components (laser, fiber, photodiode, MZM and VOA) which are needed

to the systems in analysis. In the electrical field, some focus has been given to the modulation format, QAM, used in the 802.11g standard. The electric components described are the QAM transmitter and receiver, and the EVM evaluator.

In the third chapter, RoF is widely described, from its concept to the developments made until today, as well as the implementation areas. Furthermore, it is presented the analog optical links concept, with the two possible scenarios for RoF systems implementation: direct and external modulation.

The fourth chapter presents, first, the analysis of the correction factor for the power estimation, and secondly, the setups used to verify the reliability of the implemented models, as well as the results and their discussion.

Finally, the chapter five presents briefly the main conclusions of the work described in this dissertation, and the future directions to be taken, from the developed work presented.

1.4 Main Contributions

The first main contribution of this work is the deduction of a correction factor used in the power estimation of QAM finite sequences, fundamental to proceed with the simulations. From this derivation it was submitted a paper to SEONs - Symposium of Enabling Optical Networks and Sensors:

- H. L. Moura, Paulo P. Monteiro, Rui S. Ribeiro, "Power Estimation and EVM Evaluation of QAM Finite Sequences," *SEON's*, 2009.

The other contribution is the implementation of models required to make possible RoF systems analysis in OSIP software, particularly the Signal Generator, the Signal Receiver and EVM Evaluator in electrical domain, and, in optics, the DFB laser rate equations model to enable direct modulation RoF schemes.

2

Background Material

2.1 Optical Transmission

2.1.1 Single Mode Fiber

Refractive index is the ratio of the speed of light in a vacuum to the speed of light in that material [1].

The optical fiber is a dielectric optical waveguide, which consists of a cylindrical core surrounded by a cladding layer and the set is protected by a jacket, as shown in Figure 2.1. The core and the cladding are both made primarily of silica (SiO_2) and are designed so the core presents a higher refractive index than the cladding. This technique is essential to confine the propagating light in the core. Albeit there are two kinds of fibers, the Single Mode Fiber (SMF) and the Multi-Mode Fiber (MMF), this text will only focus the former,

the SMF. Single-Mode Fibers (SMF) supports only the fundamental mode, and this is achieved by reducing the core radius so that only the mode with a 90º angle of incidence with the interface air/core propagates trough the core.

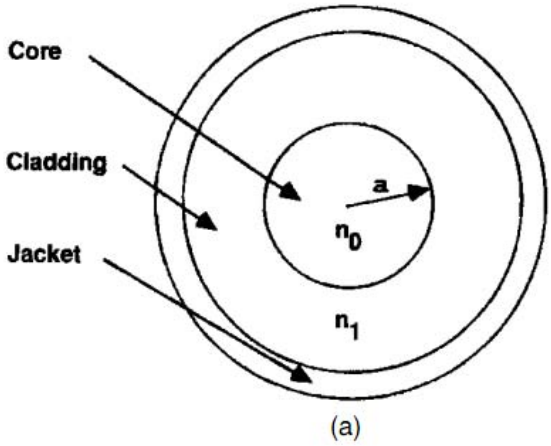

Figure 2.1 –Optical fiber structure. n_1 – core refractive index; n_2 – cladding refractive index; a – core radius.

2.1.1.1 Attenuation

Just like in all transmission mediums known, attenuation is also a fundamental characteristic in optical fiber domain. It is an important factor to consider when determining the maximum distance possible of optical signal propagation, for particular transmitter power and receiver sensitivity (minimum power required in the receiver to detect the signal).

The optical signal power at the end of an L km length optical fiber, P_L is:

$$P_L = P_0 \exp(-\alpha L) \tag{2.1}$$

where P_0 is the optical power in the transmitter , and α is the attenuation coefficient. Usually, the attenuation of a fiber is referred in (dB/km), by [2]:

$$\alpha\left(dB/km\right) \approx 4,343\alpha \tag{2.2}$$

Figure 2.2 shows the loss spectrum of a Standard SMF. It shows the fiber attenuation as a function of optic signal wavelength.

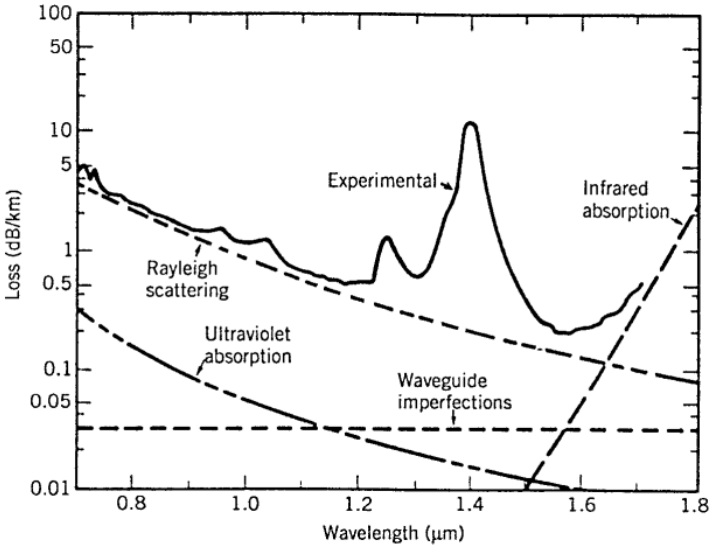

Figure 2.2 - Loss spectrum of a single-mode fiber produced in 1979. (After [2])

Several factors contribute to attenuation, which can be divided into two categories: absorption and scattering.

2.1.1.2 Absorption

There are two major components in absorption losses, intrinsic and extrinsic. The former are related to the absorption by the basic constituent material of the fiber (usually silica – SiO_2). Figure 2.2 shows that intrinsic absorption over the entire 0.8-1.6μm is negligible. The electronic resonances of SiO_2 occur in the ultraviolet region ($\lambda < 0.4$ μm), whereas vibrational resonances occur in the infrared region ($\lambda > 7$ μm) [2]. So, intrinsic absorption defines the spectral window accessible for optical communications. Extrinsic absorption is due to impurities of the optical fiber. Most of these impurities are residual water vapors, which are responsible for the attenuation peaks in the 0.95, 1.24 and 1.39μm, due to OH ion vibrational resonance [2].

2.1.1.3 Scattering

During fiber manufacturing, it is impossible to produce a perfect, homogeneous thread of silica. Therefore, small variations in the material density lead to random fluctuations of the refractive index. This is the fundamental factor of losses by scattering and is known as Rayleigh scattering. The attenuation coefficient decreases highly with the increase of the wavelength by [2]:

$$\alpha_R = C_R / \lambda^{-4} \tag{2.3}$$

where C_R is the Rayleigh coefficient.

The loss related to Rayleigh scattering is the dominant component of losses in today's fibers in all the three wavelength bands used for optical communication: 0.8μm, 1.3μm, and 1.55μm.

2.1.1.4 Chromatic Dispersion

Dispersion is referred when different components of the transmitted signal have different velocities and, as result, they don't arrive at the same time at the receiver [3]. Chromatic dispersion, also known as the group-velocity dispersion (GVD) or intramodal dispersion, has two contributions: the material dispersion and the waveguide dispersion.

The material dispersion is related to the fact that the refractive index of silica is dependent on the operating frequency. Therefore, the effect of the distortion on the signal is proportional to the optical signal bandwidth so a wider spectral bandwidth will be more affected by the material dispersion. It can be quantified in [ps/nm.km] by [2]:

$$D_m = -\frac{\lambda_0}{c}\frac{d^2 n_1}{d\lambda_0^2} \tag{2.4}$$

The waveguide dispersion, in the other way, is related with the confinement of the wave into the core. The electric field inside the fiber don't travel restricted to core medium. Larger wavelengths will propagate less confined in the core, and more energy will propagate in the cladding, just like is depicted in the Figure 2.3. Its effective index will be smaller [3], and as the velocity is inversely proportional to refractive index, the larger wavelengths will propagate faster.

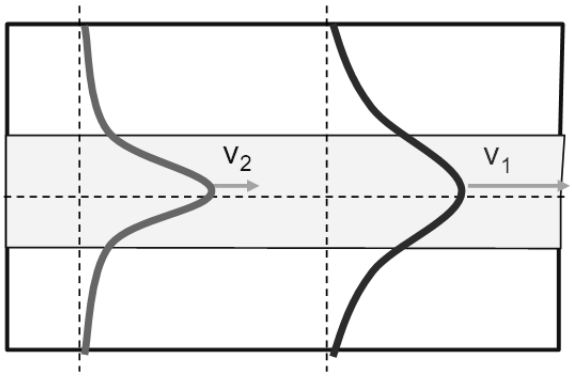

Figure 2.3 – Electric field confinement in optical fiber. V_1 and V_2 correspond to a larger and a smaller wavelength wave, respectively.

The waveguide dispersion can be derived [2] and modeled by:

$$D_w = -\frac{n_1 \Delta}{c\lambda_0} V \frac{d^2(bV)}{dV^2} \tag{2.5}$$

where c is the light velocity in vacuum, n_1 is the refractive index of the core, λ_0 is the wavelength of the optic wave, Δ is the fractional index change and the other term can be approximated analytically by:

$$\frac{d^2(bV)}{dV^2} \approx 0.080 + 0.549\left(2.834 - V\right)^2, 1.4 < V < 2.6 \tag{2.6}$$

$$V = \frac{2\pi a}{\lambda_0}\sqrt{n_1^2 - n_2^2} \tag{2.7}$$

Figure 2.4 shows total chromatic dispersion, as well as both contributions of material and waveguide dispersion.

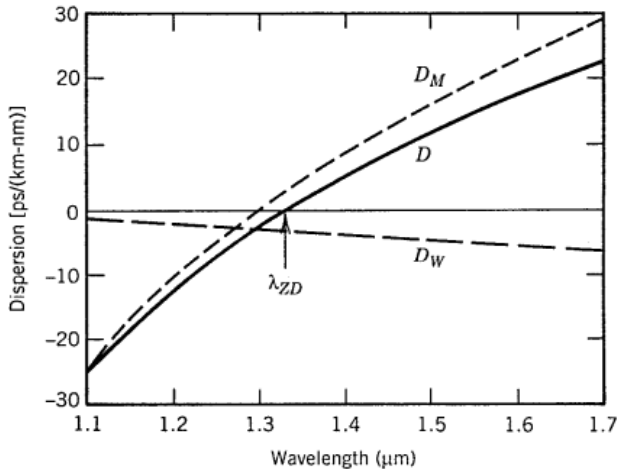

Figure 2.4 – Total dispersion and relative contributions from material and waveguide dispersion. λ_{ZD} is the wavelength where fiber presents zero dispersion.(After [2]).

2.1.2 Laser

The term laser is an acronym for light amplification by stimulated emission of radiation. The emitted radiation has spatial and temporal coherence, which means that the light beam has low spectral width and is very directional. This results in high coupling efficiency to optical fiber. Laser diodes can, additionally, produce high output optical power.

The structure of a laser is shown in Figure 2.5. It is obtained from an excitation device, a Fabry Perot cavity formed by two reflective facets (one of them is not totally reflective, to produce an output light beam) and a gain or lasing medium, which can be a gas, a liquid, an insulating crystal, or a semiconductor. This latter material is, by far, the most used in light sources of today's optical communication systems.

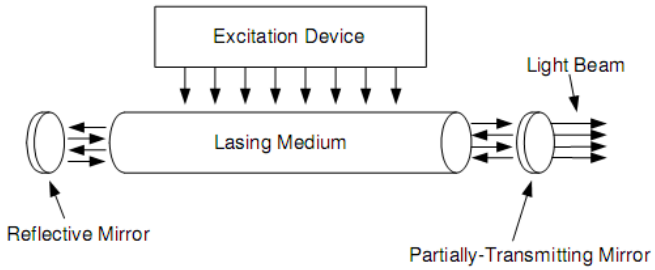

Figure 2.5 – Structure of a laser

Excitation device provides electrons to start the lasing process. The lasing medium provides optical amplifying, and the reflective mirrors turn the laser into an oscillator. One of them is partially transmitter, to permit the light radiation.

The principle of operation of any laser, regardless of its medium material, results from three basic processes: photon absorption, spontaneous emission and stimulated emission, as shown in Figure 2.6. E_1 and E_2 corresponds to electron energy state levels, ground- and excited-state levels, respectively [1].

The first process, photon absorption (Figure 2.6 – (a)) describes the transition of an electron from E_1 to E_2. This transition occurs when an electron absorbs energy from a nearby passing photon of energy $E_{12}=E_2-E_1$. In the excited-state, the electron is unstable, and will return quickly, without external stimulation, to ground-state, thereby emitting a photon of energy E_{12}. In this process, referred as spontaneous emission (Figure 2.6 – (b)), there is isotropic and of random phase light emission.

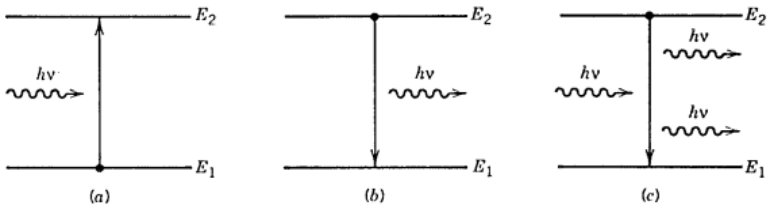

Figure 2.6 - Laser basic processes. (a)-photon absorption, (b)-spontaneous emission and (c)-stimulated emission. [2]

When a photon impinges in the material while the electron is in the excited state, it will stimulate the electron to transit to ground-state, releasing a photon of energy $E_{12}$with the same phase and direction of the stimulating photon. This process is known as stimulated emission (Figure 2.6 – (c)).

Since spontaneous emission occurs without any external excitation, any incident photon will be immediately absorbed, producing a narrowband gaussian output. If one wants to have an optical source with stimulated emission prevalence, there is one condition to meet. In the lasing medium, the population of the excited states has to be higher than the population in the ground state. This condition is known as the population inversion. But, this condition can only be satisfied with external stimulating techniques.

With population inversion, one spontaneous photon will trigger a chain of stimulated photons (by the process of stimulated emission) exhibiting optical gain, g_m, inside the laser. The lasing medium is therefore an optical amplifier. The lasing process in a semiconductor laser is stimulated by electric current from the excitation device, and requires not only optical gain in the lasing medium, but also optical feedback, which is guaranteed by the reflecting mirrors. They are, albeit, dispensable in the semiconductor laser once its two cleaved facets replace them. Their reflectivity is given by [2]:

$$R_m = \left(\frac{n_l - 1}{n_l + 1} \right)^2 \tag{2.8}$$

where n_l is the refractive index of the lasing medium. The reflective facets will provide strong optical feedback, thus converting the device into an oscillator with a gain mechanism that compensates for optical losses in the cavity (lasing medium). In semiconductors, from the moment that population inversion is realized, the optical gain increases rapidly [2].

In the lasing process there are losses due to absorption and others (in the mirrors, material dispersion and non-radiative processes), and with low carrier density, the optical gain may not be sufficient to produce an optical output. Hence, there is a minimum of current needed to compensate the losses, and it is defined as the *current threshold* (I_{th}). Related to this is the lasing-threshold optical gain, which is defined by the minimum gain needed to overcome the losses, which is [2]:

$$g_{th} = \alpha_i + \alpha_{mirror} = \alpha_i + \frac{1}{2L_c} \ln\left(\frac{1}{R_{m1}R_{m2}}\right) \tag{2.9}$$

where α_i is the intrinsic losses in the lasing medium, and α_{mirror} refers to losses in the mirrors. L_c is the length of the cavity.

Laser cavity may have several resonant frequencies. By the phase condition [1],

$$m = \frac{L_c}{\lambda / 2n_l} \tag{2.10}$$

are the longitudinal modes of the laser, the wavelengths that are induced in the cavity from the oscillation. The separation between consecutive modes is:

$$\Delta\lambda = \frac{\lambda^2}{2L_c n_l} \tag{2.11}$$

or in frequency:

$$\Delta f = \frac{c}{2L_c n_l} \tag{2.12}$$

Laser gain is a function of frequency and not all the modes can satisfy the gain condition (g_{th}). This relation can be described by a gaussian law [2]:

$$g(\lambda) = g(0)\exp\left(-\frac{(\lambda - \lambda_0)}{2\sigma^2}\right) \tag{2.13}$$

where λ_0 is the wavelength at the center of the spectrum, σ is the spectrum width of the gain, and $g(0)$ is proportional to population inversion. In Figure 2.7 is shown the gain versus frequency of a semiconductor laser.

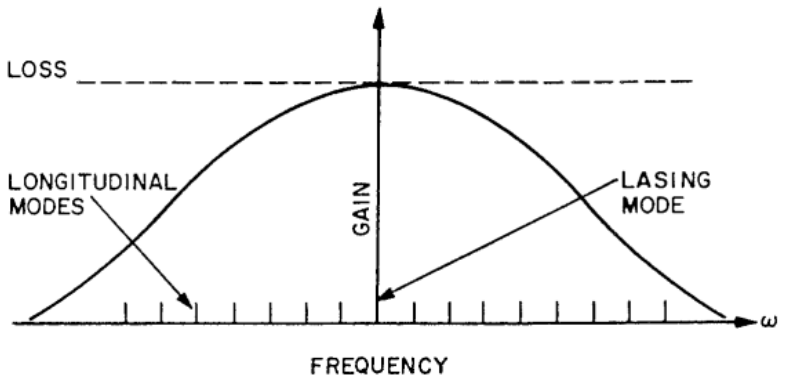

Figure 2.7 - Gain and loss profiles in semiconductor lasers. Vertical bars show the location of longitudinal modes. After [2].

In a single-mode laser, the only mode that verifies (equação g_{th}) is the center mode, which is the only mode that guarantees the gain threshold. In opposite, in a multi-mode laser, other modes satisfy the gain threshold and several modes will be emitted.

2.1.2.1 Distributed Feedback (DFB) Laser

One way to produce single-mode lasers (only one longitudinal mode falls in the gain bandwidth of the device) is to reduce the cavity length *L* so that the frequency separation increases so that other modes do not appear within the gain window that overcomes the losses and will vanish.

The distributed feedback laser (DFB) is built-in with a frequency selective resonator grating. The operation of this laser configuration is based on the distributed Bragg phase-grating reflector which leads to a periodic variation of the mode index.

The structure of a DFB is shown in Figure 2.8. The feedback is not provided by the lateral facets, but from the grating through the lasing medium. The phenomenon which permits this condition is the Bragg diffraction. The wave modes traveling both forward and backward direction will undergo successive reflections. Consider the following Bragg condition, where λ_B is the Bragg wavelength, Λ is the granting period, m_B is the diffraction order and $\bar{n}$ is the average mode index [1-2].

$$\Lambda = m_B \frac{\lambda_B}{2\bar{n}} \tag{2.14}$$

The reflected waves will add in phase if the Bragg condition is satisfied. The maximum coupling possible will be possible for $m_B=1$. They are usually used to suppress

all the longitudinal modes, except the one that his wavelength equals (or is the closest) twice the grating period.

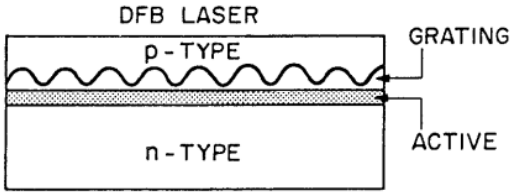

Figure 2.8 - DFB laser structure. After [2]

DFB lasers have low sensitivity to drive-current and temperature variations [1].

2.1.2.2 Rate equations

The behavior of a single-mode laser can be modeled by three equations, based in classic mechanics, known as the semi-classic model [4].

Classic mechanics gives the physical phenomena approach, but it lacks in modeling the noise from the random nature of spontaneous emission neither and from carriers discrete nature. In this method this noise is considered by adding noise sources to the three equations.

2.1.2.3 Populations Rate Equations

The non-linear, differential equations, are the rate equations, and expressing them in order to populations take the form [4]:

$$\frac{dN_p(t)}{dt} = \frac{I(t)}{q} - \frac{N_p(t)}{\tau_n} - g_p(t)S_p(t) + f_{np}(t) \tag{2.15}$$

$$\frac{dS_p(t)}{dt} = g_p(t)S_p(t) - \frac{S_p(t)}{\tau_p} + \beta_s \frac{N_p(t)}{\tau_n} + f_{sp}(t) \tag{2.16}$$

$$\frac{d\phi(t)}{dt} = \frac{\alpha_H}{2} g_{po}\left[N_p(t) - N_{pt}\right] + f_\phi(t) \tag{2.17}$$

The $S_p(t)$ and $N_p(t)$ are the photon and carrier populations, $\phi(t)$ is the electric field phase, $I(t)$ is the injection current, τ_p is the photon lifetime and τ_n is the carrier lifetime, β_s is the spontaneous emission factor. N_{pt} is the transparency value of the carrier population,

α_H is the linewidth enhancement factor, and q is the known charge of an electron. $f_s(t)$, $f_n(t)$ and $f_\phi(t)$ are Langevin noise sources that model the above described noise factors.

$g_p(t)$ is the stimulated emission gain for populations, given by:

$$g_p(t) = g_{po} \frac{N_p(t) - N_{pt}}{1 + \varepsilon_p S_p(t)} \tag{2.18}$$

where ε_p is proportional to the nonlinear gain ε by:

$$\varepsilon_p = \frac{\Gamma}{V_a} \varepsilon \tag{2.19}$$

and g_{po} is related to the differential gain g_o by:

$$g_{po} = \frac{\Gamma}{V_a} g_o \tag{2.20}$$

Γ is the confinement factor and V_a is the active layer volume. The differential gain g_o is:

$$g_o = g_m v_g \tag{2.21}$$

where g_m is the linear material gain coefficient and v_g is the group velocity.

Both two next definitions express respectively the carrier and photon populations in order to their densities:

$$N_p(t) = V_a N(t) \tag{2.22}$$

and

$$S_p(t) = \frac{V_a}{\Gamma} S(t) \tag{2.23}$$

The transparency value for carrier population is given by:

$$N_{pt} = V_a N_t \tag{2.24}$$

The optical power is related to photon density, and it is given by:

$$P(t) = \frac{\eta h\nu}{\tau_p} S_p(t) \tag{2.25}$$

where h is the Planck constant, ν is the optical frequency and η is the quantum efficiency of the intrinsic laser.

2.1.2.4 Bias Point

The threshold current can be obtained from:

$$I_{th} = \frac{q}{\tau_n}\left(N_{pt} + \frac{1}{g_{po}\tau_p} \right) \tag{2.26}$$

We have to obtain the operation point of the laser, to start modeling the laser. It is related to the mean value of the input current I_0, which has to be higher than the current threshold.

The carrier and photon population densities obtained from [4]:

$$\begin{cases} \frac{I_0}{q} - \frac{N_{po}}{\tau_n} - g_{po}\frac{N_{po} - N_{pt}}{1 + \varepsilon S_{po}} S_{po} = 0 \\ g_{po}\frac{N_{po} - N_{pt}}{1 + \varepsilon_p S_{po}} S_{po} - \frac{S_{po}}{\tau_p} + \beta_s \frac{N_{po}}{\tau_n} = 0 \end{cases} \tag{2.27}$$

The value of the photon density in the bias point is, then:

$$S_{po} = \frac{-b - \sqrt{b^2 - 4ac}}{2a} \tag{2.28}$$

with:

$$a = -\frac{1}{\tau_p}\left(\tau_n g_{po} + \varepsilon_p \right) \tag{2.29}$$

$$b = \frac{I_0}{q}\left(\tau_n g_{po} + \beta_s \varepsilon_p \right) - \left(1 - \beta_s \right) g_{po} N_{pt} - \frac{1}{\tau_p} \tag{2.30}$$

$$c = \beta_s \frac{I_0}{q} \tag{2.31}$$

The carrier population density at the bias point is:

$$N_{po} = \frac{\tau_n}{1-\beta_s}\left(\frac{I_0}{q} - \frac{S_{po}}{\tau_p}\right) \tag{2.32}$$

2.1.2.5 Relaxation frequencies

According to [4], the relaxation frequency of a laser is:

$$w_{rr} = \sqrt{Q_p\left(Q_n + \frac{\beta_s}{\tau_n}\right) - \frac{1}{4}\left(\gamma_n - \gamma_p\right)^2} \tag{2.33}$$

where Q_p, Q_n, γ_p, γ_p are given by [4]:

$$Q_n = \frac{g_{po} S_{po}}{1+\varepsilon_p S_{po}} \tag{2.34}$$

$$Q_p = \frac{g_{po}(N_{po} - N_{pt})}{(1+\varepsilon_p S_{po})^2} \tag{2.35}$$

$$\gamma_n = \frac{1}{\tau_n} + Q_n \tag{2.36}$$

$$\gamma_p = \frac{1}{\tau_p} - Q_p \tag{2.37}$$

2.1.2.6 Amplitude and frequency response of the DFB laser

The amplitude response of a DFB laser is given by [4]:

$$H_A(\omega) = \frac{\eta h\nu}{\tau_p} \cdot \frac{K_0}{(A_0 - \omega^2) + j\omega A_1} [W/Hz] \tag{2.38}$$

and the frequency response is [4]:

$$H_F(\omega) = \frac{\alpha_H g_{po}}{4\pi q} \cdot \frac{\frac{1}{\tau_p} - Q_p + j\omega}{(A_0 - \omega^2) + j\omega A_1} [Hz/mA] \tag{2.39}$$

where A_0, A_1 and K_0 are given by:

$$A_0 = \frac{1}{\tau_p}\left(\frac{1}{\tau_n} + Q_n\right) - \left(1-\beta_s\right)\frac{Q_p}{\tau_n} \tag{2.40}$$

$$A_1 = \frac{1}{\tau_p} + \frac{1}{\tau_n} + Q_n - Q_p \tag{2.41}$$

$$K_0 = \frac{1}{q}\left(Q_n + \frac{\beta_s}{\tau_n}\right) \tag{2.42}$$

2.1.2.7 Lowpass Equivalent CW Laser

Continuous Wave (CW) lasers are generally used when there is an external modulator device to modulate the electric signal. They are characterized by a narrow linewidth, and permit to reduce largely the chirp, depending on the modulators used. The optical field produced by the laser can be written as:

$$E_{CW}(t) = Ae^{j(w_0 t + \phi + N_{FM}(t))} \tag{2.43}$$

One can use the lowpass equivalent to express the output signal of a CW laser:

$$E_{lpCW}(t) = \frac{A}{\sqrt{2}} e^{j(\phi + N_{FM}(t))} \tag{2.44}$$

where A is the amplitude, w_0 is the optical frequency, ϕ is the initial phase and $f_n(t)$ is the frequency modulation due to noise. Linewidth is related to this latter parameter.

2.1.3 Photodiode *p-i-n*

The photodiode is a transducer, which takes place at the output of the optical transmission line. The photodiode converts the incident light (optical signal) in electric current.

In this text the approach will focused in semiconductor *pin* photodiodes. Their structure is composed by a *pn* junction with an intrinsic layer, *i*, just as the Figure 2.9 shows [1].

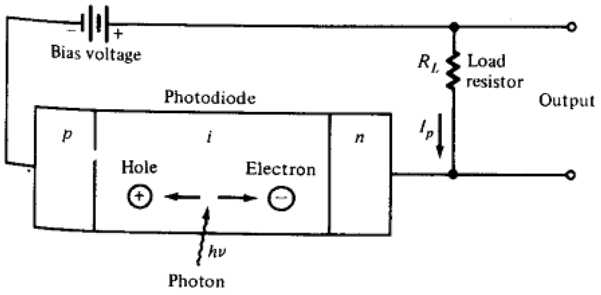

Figure 2.9 – *p-i-n* photodiode schematic. The photon appears to be inciding the intrinsic layer, but the scope of the draw is to show that most of the photon incide in this layer. The photons incide longitudinaly in the photodetector and most of them are absorbed in the intrinsic layer.

The middle layer (*i*) is formed by a lightly doped semiconductor material and it is used to increase the depletion region (*pn* junction). A large reverse-bias voltage is applied across the device so that the intrinsic layer have a greater impurity concentration when compared to *n* and *p* regions, which in turn results in an improvement of the responsivity of the photodiode [3].

The Figure 2.10 shows the energy-band diagram of a *pin* photodiode. There is a voltage drop between *p* and *n* regions, due to the reverse-bias voltage.

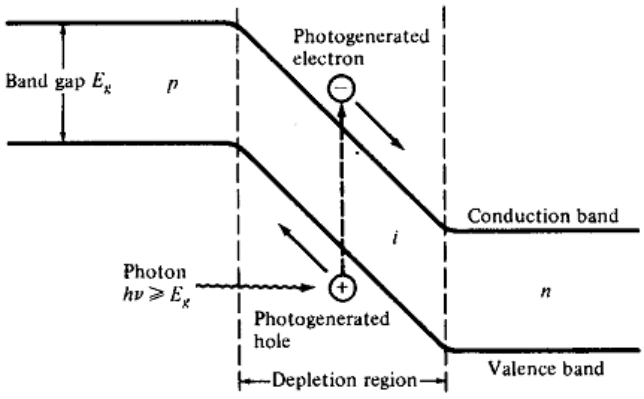

Figure 2.10 - Energy-band diagram of a *pin* photodiode

Incident photons will excite electrons from the valence band to the conduction band if its energy is at least equal to the band-gap energy *hv* of the semiconductor material. This process generates electron-hole pairs known as *photocarriers* [1]. This process occurs essentially in the intrinsic depletion region, where most of the light is absorbed. Due to the reverse-biased voltage applied to the *pn* junction, the photocarriers will flow (electrons from the valence band to the *n* region and holes to the *p* region) and produce the *photocurrent*. The intrinsic region improves the operation of the photodiode by making the

drift current (due to the photon absorption and the electric field imposed by the reverse bias voltage) dominate over the diffusion current (related to the movement of the electrons/holes naturally by their charge).

The photocurrent I_{pin} is directly proportional to the incident optical power P_{pin} by [2]:

$$I_{pin} = RP_{pin} \tag{2.45}$$

where R is the responsivity of the photodetector:

$$R = \frac{\eta q}{h\nu} \approx \frac{\eta \lambda}{1.24} \tag{2.46}$$

where η is the quantum efficiency. One can see that the responsivity increases with the wavelength, this is because the incident light, with the same optical power, carries more photons, but each one of them with a little less energy. The limit is for the wavelength with photons with less energy than the semiconductor band gap.

2.1.4 Mach-Zehnder Modulator

The Mach-Zehnder Modulator (MZM) is usually used as the optic modulator in external modulation schemes. It is an intensity modulator, and can be achieved with two phase modulators (the) and two $3dB$ couplers [3], as presented in Figure 2.11.

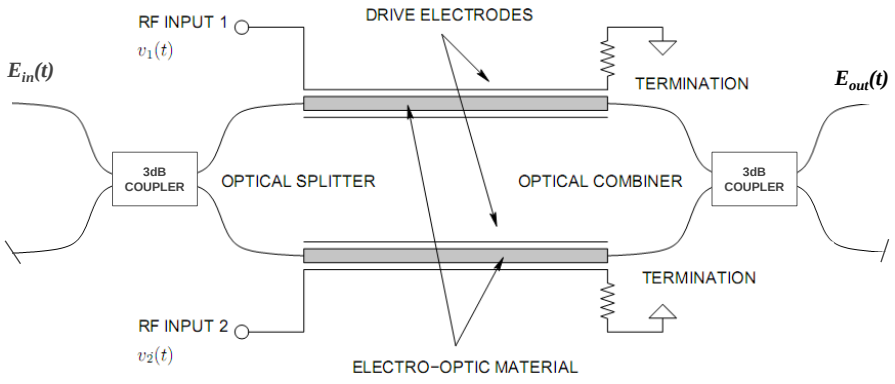

Figure 2.11 – Mach-Zehnder Modulator

Each phase modulator is based in the Pockels effect, also known as the linear electro-optic effect, which is a phenomenon in which the refractive index of a medium varies linearly with the application of an electric field [5]. This phenomenon occurs only in non-

centrosymmetric materials, such as lithium niobate ($LiNbO_3$), lithium tantalate ($LiTaO_3$) and gallium arsenide (GaAs).

The input CW beam is split in the 3*dB* coupler to each arm, and after phase modulation in each arm, both waves are recombined back by another 3*dB* coupler. Depending on the voltage $v(t)$ across the electro-optic material, the optical filed will undergo a phase shift of [6]:

$$\theta_{MZM}(t) = \theta_0 - \pi \frac{v(t)}{V_\pi} \tag{2.47}$$

where θ_0 is the phase change in the electro-optic material, and V_π is the voltage needed to introduce a phase shift of 180º into the input optic wave. It is usually a characteristic of the modulator.

With the push-pull configuration, the bias voltage is given by

$$V_M = V_1 - V_2 \tag{2.48}$$

where V_1 is the mean value of $v_1(t)$, and V_2 is the mean value of $v_2(t)$.

Let us analyze the influence of the MZM in the electric field intensity, taking into account the MZM schematic in Figure 2.11.

Consider the 3dB coupler shown in the Figure 2.12, with coupling ratio α_{3dB}.

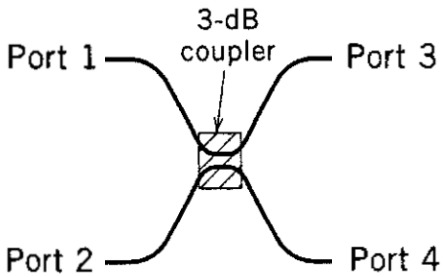

Figure 2.12 – 3dB coupler.

At the ports 3 and 4 the optical field is:

$$E_3(t) = \sqrt{\alpha_{3dB}} E_1(t) + \sqrt{1-\alpha_{3dB}} E_2(t) \tag{2.49}$$

$$E_4(t) = \sqrt{1-\alpha_{3dB}}E_1(t) + \sqrt{\alpha_{3dB}}E_2(t) \tag{2.50}$$

Each arm will produce a phase shift of:

$$\theta_{MZM\_1}(t) = \theta_0 - \pi\frac{v_1(t)}{V_\pi} \tag{2.51}$$

$$\theta_{MZM\_2}(t) = \theta_0 - \pi\frac{v_2(t)}{V_\pi} \tag{2.52}$$

With α_{3dB}=0.5, the power of the incident wave is equally divided to both arms in the first coupler, and is recombined back in the second. The output optical field in MZM is:

$$E_{MZM\_out}(t) = \frac{1}{A_{tt}}\left(\frac{\sqrt{2}}{2}e^{j\theta_{MZM\_1}(t)}\frac{\sqrt{2}}{2} + \frac{\sqrt{2}}{2}e^{j\theta_{MZM\_2}(t)}\frac{\sqrt{2}}{2}\right)E_{MZM\_in}(t) \tag{2.53}$$

$$E_{MZM\_out}(t) = \frac{E_{MZM\_in}(t)}{A_{tt}2}\left(e^{j\theta_{MZM\_1}(t)} + e^{j\theta_{MZM\_2}(t)}\right) \tag{2.54}$$

where A_{tt} is the attenuation due to the insertion losses, inherent of each MZM.

2.1.5 Variable Output Attenuator

Optical attenuators are passive optical components that can reduce optical power propagating in optical fibers, and may be categorized as either fixed or variable attenuators.

In ligthwave communication systems, the use of VOAs is very important to control the light intensity at some points of the system. For instance, they are used to prevent damages due to irregular optical variations.

The VOA makes use of a feedback control loop, and an output power detector, to maintain the optical power relatively constant.

2.2 Electrical Signals

2.2.1 Quadrature Amplitude Modulation

Quadrature Amplitude Modulation (QAM) technique is an example of Mary signal transmission in which *k* successive binary digits are used to produce one of the $M=2^k$ waveforms possible to be transmitted. This technique increases the spectral efficiency since several bits are encoded into one symbol, but also is more sensible to noise [7].

QAM may be viewed as form of combined digital amplitude and phase modulation. The bandpass waveform can be written as [8]:

$$v_{bp}(t) = A(t)\cos(w_c t + \theta_e(t)) = v_i(t)\cos(w_c t) - v_q(t)\sin(w_c t) \quad (2.55)$$

with $v_i(t) = A(t)\cos(\theta_e(t))$, $v_q(t) = A(t)\sin(\theta_e(t))$ and w_c is the carrier frequency. $A(t)$ is the envelope and $\theta_e(t)$ the phase, both functions of time. As we can see, $v_{bp}(t)$ has the contribution of two phase-quadrature carriers.

The QAM modulation involves two orthogonal passband basis functions [9]:

$$\varphi_1(t) = \sqrt{\frac{2}{T}}\cos(w_c t) \qquad ,0 \le t \le T; \quad (2.56)$$

$$\varphi_2(t) = -\sqrt{\frac{2}{T}}\sin(w_c t) \qquad ,0 \le t \le T; \quad (2.57)$$

where T is the period of each symbol. The amplitude normalization $\sqrt{2/T}$ guarantees orthonormality between the carriers.

Consider the particular signal-space diagram in the $(\varphi_1(t), \varphi_2(t))$ plane presented in Figure 2.13, which is a 64-QAM (M=64), where the M symbols are mapped by a user-specified rule, which has to be the same in modulator and demodulator.

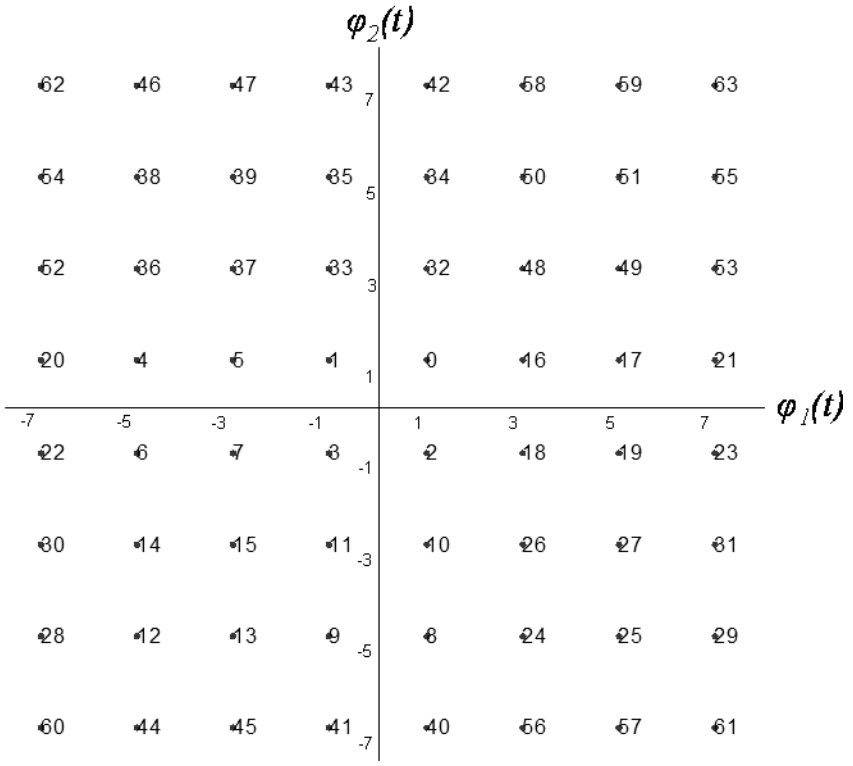

Figure 2.13 – Signal-space diagram

Each symbol/point is denoted by $s_k \to (a_k d_{\min}/2; b_k d_{\min}/2)$, $k = 1,2,...,M$; $a_k, b_k \in \{-7;-5;-3;-1;1;3;5;7\}$, and $d_{\min}$ is the minimum distance between two neighbor points. The energy of the lowest amplitude symbols can be related to $d_{\min}$ by:

$$E_0 = \int_0^T s_0^2(t)dt = \int_0^T \left(\frac{d_{\min}}{2}\varphi_1(t) + \frac{d_{\min}}{2}\varphi_2(t) \right)^2 dt \tag{2.58}$$

$$E_0 = 2\left(\frac{d_{\min}}{2}\right)^2 \tag{2.59}$$

So, the bandpass waveform of the k-th symbol can be written as [9]:

$$s_k = \sqrt{\frac{E_0}{T}} a_k \cos(w_c t) - \sqrt{\frac{E_0}{T}} b_k \sin(w_c t), 0 \le t \le T, k \in \mathbb{Z} \tag{2.60}$$

The previous signal is related to E_0, but a more convenient approach is to write it in order to the signal average power P_{av} (considering identically distributed symbols), which is proportional to the average energy by $E_{av}=P_{av}T$.

For a square constellation like the one in Figure 2.13, the average energy is related [9] to E_0 by $E_{av} = \frac{(M-1)E_0}{3}$ from which:

$$s_k = \sqrt{\frac{3P_{av}}{M-1}} a_k \cos(w_c t) - \sqrt{\frac{3P_{av}}{M-1}} b_k \sin(w_c t),\ 0 \le t \le T, k \in \mathbb{Z} \tag{2.61}$$

The QAM signal, with N symbols length, can therefore be written by:

$$v_{RF}(t) = \sum_{k=0}^{N-1} s_k, \qquad k \in \mathbb{Z} \tag{2.62}$$

The QAM signal is centered in the carrier frequency, but what about the bandwidth it requires?

As in any signal, the bandwidth is equal to the baud rate. In QAM signaling it depends on the parameter M. The bandwidth can be given by:

$$BW(Hz) = \frac{Bitrate}{M}$$

2.2.2 QAM Transmitter

To generate QAM signals, a possible transmitter is the one shown in Figure 2.14. The source signal is a digital binary signal, which is mapped into symbols using, as reference, the space diagram shown in Figure 2.13. Both coordinates of each symbol will be multiplied by the respective carriers, producing the inphase and quadrature terms. They are then combined to form the waveform described in eq (2.62). The carriers used are the referred in eq (2.56) and eq (2.57).

The transmitted signal has two carriers mixed out. They will not interfere since they are orthogonal, therefore independent from each other [7].

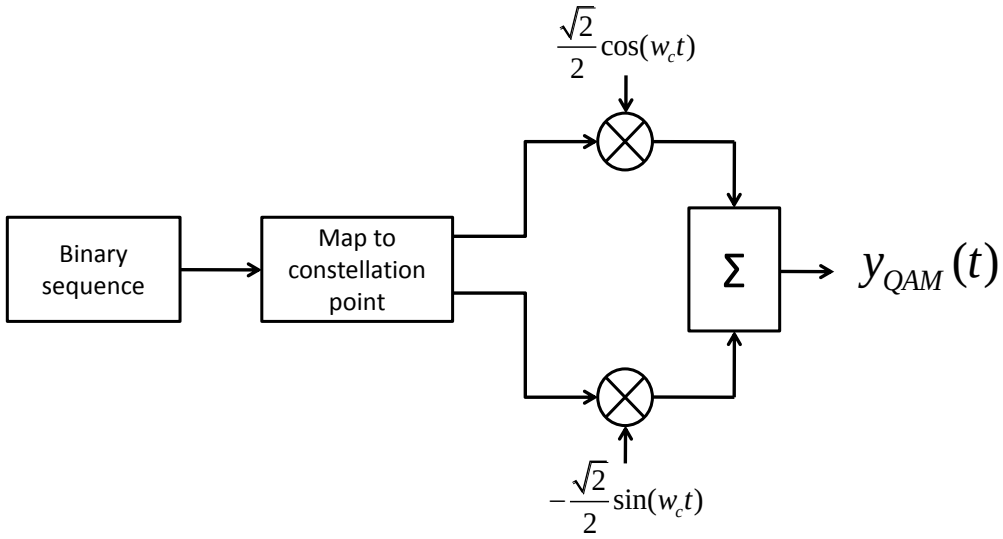

Figure 2.14 – QAM transmitter

2.2.3 QAM Receiver

The receiver is a coherent receiver (Figure 2.15). The received signal is multiplied by both of the carriers used in the transmitter, shifting the signal to baseband and separating the inphase and quadrature coordinates. The integration is performed over each symbol period.

In an ideal communication system where no noise or other impairment are considered, the output of the block "Integrate and dump" would be the transmitted coordinates. Taking into account these impairments, and depending on their magnitude, the obtained coordinates in the receiver are spaced from the original ones. Therefore a processing unit is needed to calculate the most likely symbol that was transmitted. This is the function of the Optimum Processor in Figure 2.15. In [7], one can find a complete analysis of possible optimum detector schemes.

The power estimation is essentially used to eliminate the dependence of the link gain in the received signal. However, its implementation in simulation systems has some particularities. They will be analyzed in 2.2.4.

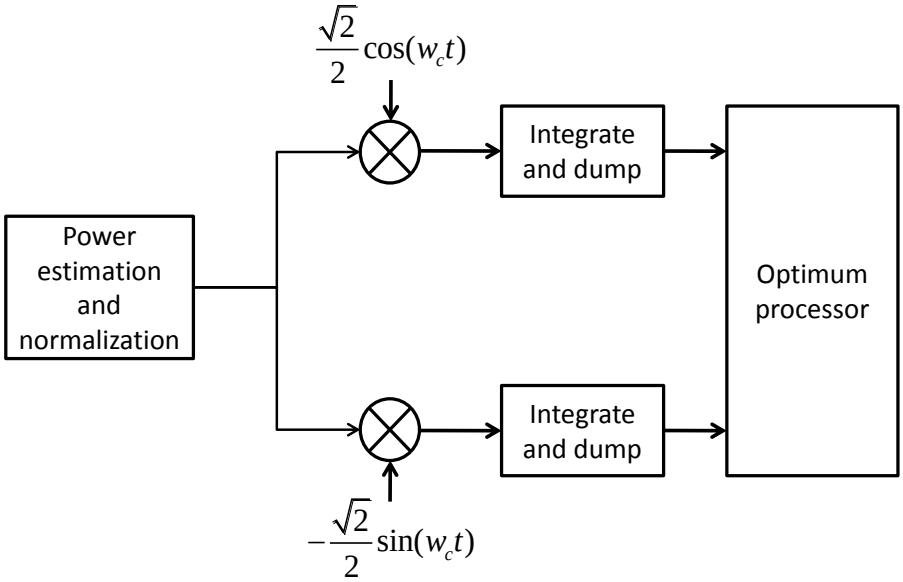

Figure 2.15 – QAM receiver

2.2.4 Power estimation of QAM finite sequences

As mentioned before, the power estimation is required for normalization purposes, so the signal received does not have the interference on the system gain distribution. Therefore, its implementation is essential to accurately estimate the transmitted symbols.

In QAM systems, the transmitted signal can be viewed as the sum of various symbols waveforms (eq (2.62)). Therefore, one can calculate the average power of each symbol, and then derive the mean for all symbols.

For one generic symbol, the average power, normalized to 1Ω, during its time interval is:

$$P_{s_k} = \frac{1}{T}\int_0^T s_k^2 t \tag{2.63}$$

$$= \frac{3P_{av}}{2(M-1)}a_k^2 + \frac{3P_{av}}{2(M-1)}b_k^2 \tag{2.64}$$

To estimate the mean power of the QAM signal ($\bar{P}$), with N symbols length, we have to obtain the mean power of all symbols:

$$\bar{P} = \frac{1}{N}\sum_{n=0}^{N-1} P_{s_n}$$

$$= \frac{1}{N}\left[\sum_{n=0}^{N-1} \frac{3P_{av}}{2(M-1)} a_n^2 + \frac{3P_{av}}{2(M-1)} b_n^2\right]$$

$$\bar{P} = \left[\frac{3}{2N(M-1)} \sum_{n=0}^{N-1} \left(a_n^2 + b_n^2\right)\right] P_{av} \tag{2.65}$$

This result shows that in multi-amplitude signaling, the power content of the signal depends not only in the average power, but also in the particular stream of the transmitted symbols. For an infinite sequence, all symbols are equally distributed and $\lim_{N\to\infty}\left[\frac{3}{2N(M-1)} \sum_{n=0}^{N-1} \left(a_n^2 + b_n^2\right)\right] = 1$, but for short symbol sequences, the energy of the individual symbols can make $\left[\frac{3}{2N(M-1)} \sum_{n=0}^{N-1} \left(a_n^2 + b_n^2\right)\right]$ to deviate significantly from the unit.

To solve the above problem, a correction factor is defined from (2.65) as:

$$S_x = \frac{3}{2N(M-1)} \sum_{n=0}^{N-1} \left(a_n^2 + b_n^2\right) \tag{2.66}$$

and estimating the coordinates a_k and b_k, it is possible to obtain the average power by:

$$P_{av} = \frac{\bar{P}}{S_x} \tag{2.67}$$

This method requires a significant level of accuracy in estimation of a_k and b_k, needing therefore large signal-to-noise ratios. Otherwise, symbols can fall in the region of adjacent ones, and estimation is not possible.

However, in simulation, the need to estimate a_k and b_k does not holds, since they can be known from the transmitter. Furthermore, this correction factor S_x acquires an extremely importance in the simulation of QAM signals with sampling frequency/transmission rate » 1, since it permits small length streams to accurate simulations, thus requiring lower processing capacity.

2.2.5 Error Vector Measurement

The Error Vector Measurement (EVM) is a measure of modulation and demodulation accuracy [10]. The system that evaluates the EVM receives the output of the integrators in Figure 2.15 which are the coordinates of the each received symbol, as can be seen in Figure 2.16.

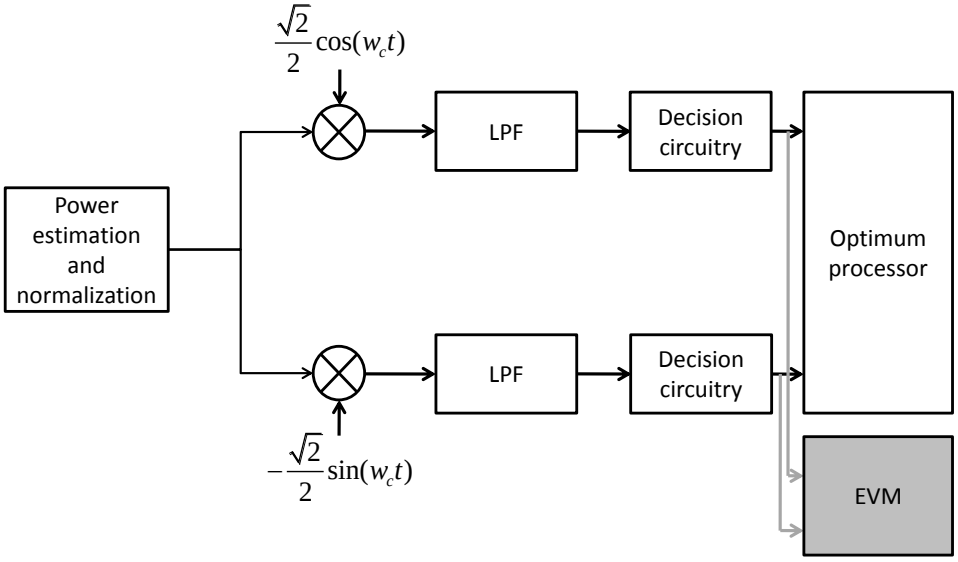

Figure 2.16 - QAM receiver with EVM evaluating block

Each measured symbol's location in the signal-space diagram $\left(I_j, Q_j\right)$ of Figure 2.13 is compared with its ideal position $\left(\bar{I}_j, \bar{Q}_j\right)$ and the EVM is then evaluated over a window of N demodulated symbols. By definition, EVM is normalized by the outermost ideal symbol's magnitude, $\left|v_{\max}\right|$:

$$EVM = \frac{\sqrt{\frac{1}{N}\sum_{j=0}^{N}\left(I_j - \bar{I}_j\right)^2 + \left(Q_j - Q_j\right)^2}}{\left|v_{\max}\right|} \tag{2.68}$$

3

Radio over Fiber

3.1 Introduction

Broadband wireless services are, today, an increasing and important sector in the telecommunications market. Fixed or mobile wireless access is viewed as an excellent way to achieve broadband services [11].

In-building coverage is one of the interest points, since it is difficult to provide effective and reliable coverage in environments as corporate office buildings, shopping malls, airports and tunnels, with only exterior antennas just as is depicted in Figure 3.1, since the successive attenuations in the concrete constructions inhibit good signal propagation. People demand more and more quality of service, particularly in terms of higher bandwidths, not to speak in the mobility and freedom, inherent to wireless systems. In those environments of high population concentration, requiring good wireless services

(cellular phones, access to internet, etc.), it is imperative to deploy an infrastructure able to provide flawless and robust services [12].

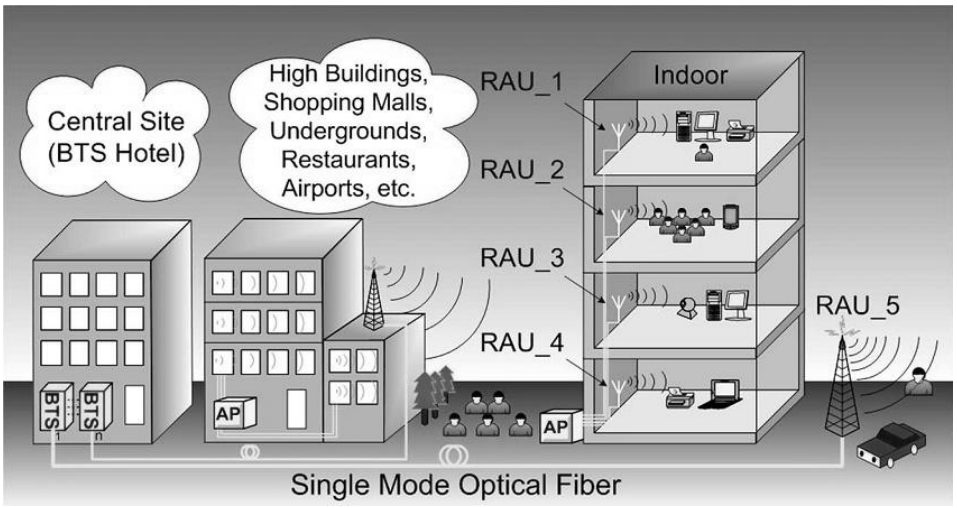

Figure 3.1 - Coverage of indoor places [13]

There are nowadays plenty of wireless standards which occupy some ranges of the frequency spectrum. For instance, the IEEE 802.11g WiFi standard offers up to 54 Mbit/s in the 2.5 and 6 GHz range; the IEEE 802.16 WiMAX standard offers up to 100 Mbit/s in the range of 10 to 66 GHz; IEEE 802.15.3 UWB operates at frequencies up to 60 GHz, offering short-range capacity up to 480 Mbit/s [14]. Figure 3.2 shows the frequency spectrum and its distribution to the communications media. Wireless communications use a range of frequencies from less than MHz to several GHz.

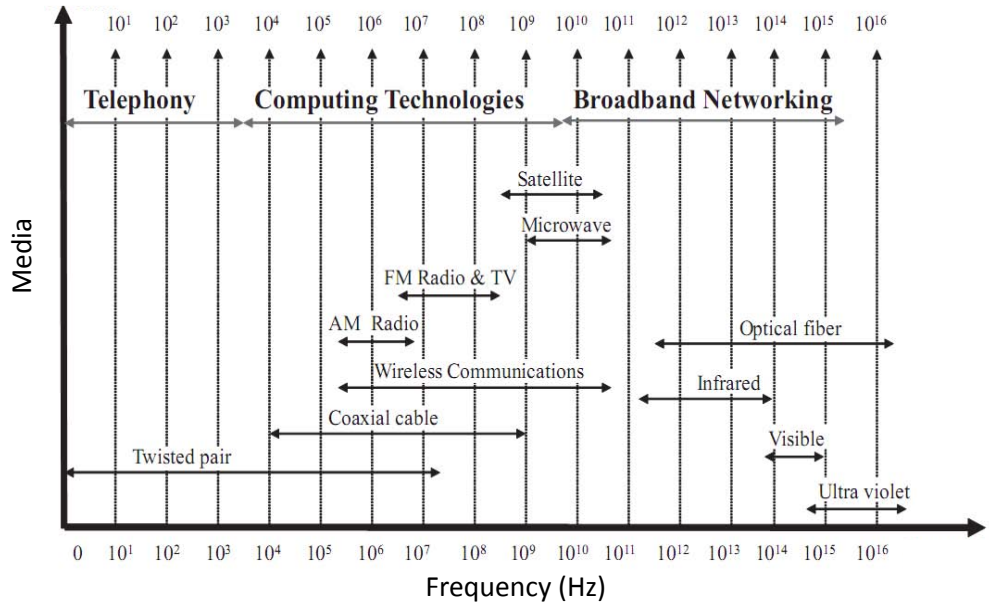

Figure 3.2 - Communications Media and Transmission Rates

By increasing the wireless capacity for each user, the wireless cells (area covered by each antenna) must be reduced, requiring many more antennas to cover a certain area. To cover environments like a hospital, for example, the number of antennas needed is very high, so one possible and economically attractive solution is to locate all the signal processing in one central office, instead of doing it in each antenna site. The transport of the processed signal could be handled by optical fiber, very suitable due to its inherent well known characteristics as very low attenuation and huge bandwidth. Therefore, the antennas only are required to do opto-electrical and electro-optical conversion, to emit and receive the wireless signal, and the microwave signal generation and modulation will therefore be transferred to the central office.

Despite of the idea being attractive at the first glance, it is attached to several constraints that inhibit its higher usage, nowadays. For instance, mainstream optical fiber technology is digital. Telecommunication networks use synchronous digital hierarchy in their cores, fiber transmission links to base stations in mobile communications systems are digital, constituting a huge part of the telecommunications and data communications market. The standardization of the digital components brought the costs down, and therefore, made the technology cheaper. At the other side, the analog optic links are present in few systems, and the technology is, hence, more expensive. In addition, analog transmission suffers from impairments such as noise and distortion that degrade the signal and cannot be regenerated [15].

This approach, even if exigent in requirements, brings flexibility, antenna site simplicity, and tailored coverage to radio networks. There is also the need to use low-cost solutions in components, to make RoF attractive. Many recent efforts have been made in R&D in optics to make RoF a success technology. A good study of low-cost picocellular architectures can be found in [16]. In terms of components, [17] presents a low-cost photodiode, [18] shows developed low-cost predistortion circuitry to compensate second- and third-order laser distortions. In optical sources, for instance, [19] presents an extremely low cost 850nm vertical-cavity surface-emitting laser (VCSEL) diode using spherical-ended multimode fiber (MMF) coupling technique. Chapter 3 of [15] is fully dedicated to low-cost solutions in RoF technology.

The idea of locate all the processing in one central office brings simplicity in system maintenance and upgrading [14]. This centralization permits the application of techniques for Multiple-Input Multiple-Output (MIMO) antenna schemes [20], mobility and connection handovers, feeding multiple radio standards [21] to an antenna reconfiguration of services to antennas, etc.

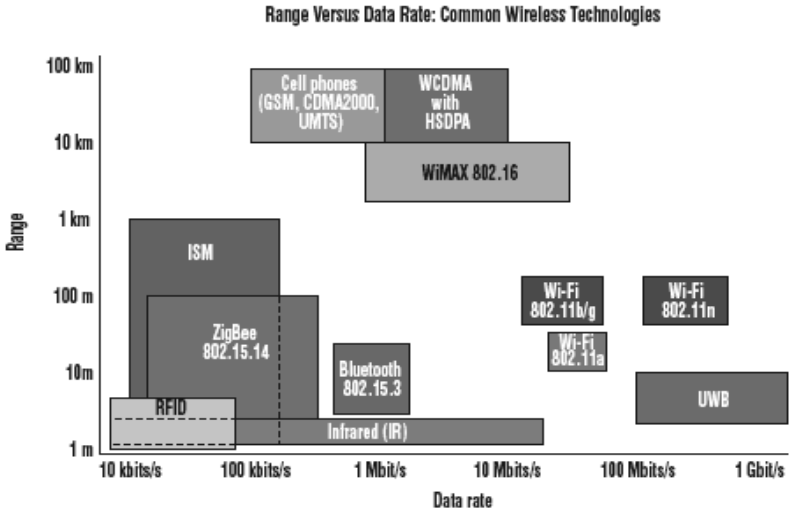

Figure 3.3 - Fixed and mobile wireless systems overview, from the point of view of data rate and mobility

3.2 What is RoF?

Radio over fiber technology gives use of the optical communications systems to transmit radiofrequency signals from a central office (CO) to the Remote Antennas Units (RAU). Actual wireless system's infrastructure is implemented within electric domain, and each base station (BS) process (frequency up-conversion, carrier modulation, and multiplexing) the signal to radiate it. The essential objective of RoF technology is to transfer all the signal processing functions to one shared location, the Central Office (CO) and then use optical fiber to transmit the signal to the RAUs as shown in Figure 3.4. Optical fiber is the ideal medium to use due to its high bandwidth and low attenuation factor (0.2dB/km in 1550 nm range and 0.5dB/km in the 1310 nm range) [22].

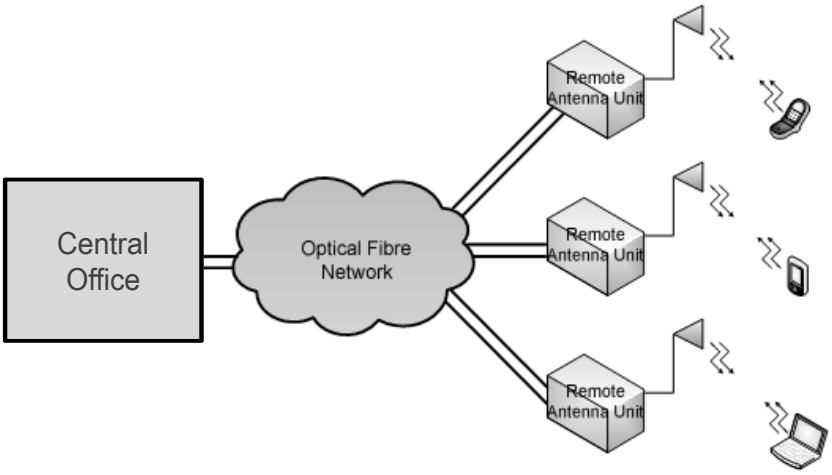

Figure 3.4 - RoF system concept

Figure 3.5 shows a basic implementation of RoF technology. It shows only the optical communication system, which is the part with most issues and with high development interest due to the importance of the system in future networks. Conceptually, the RF signal will directly modulate the laser in the central office. The optical signal will be transmitted through the fiber to the RAU and here the photodiode converts it to electric domain. Finally the electric signal will be radiated by the antenna. This is the downlink procedure. In the uplink, the antenna captures the received signal, and fed a laser, directly once more. The output signal will pass through the fiber and received by the photodiode in the CO.

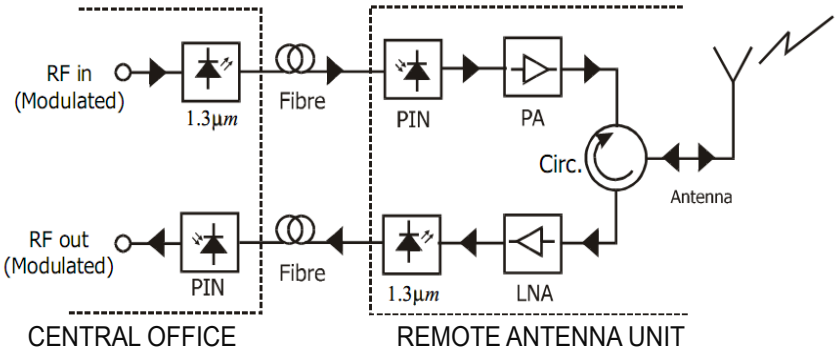

Figure 3.5 - RoF basic structure

3.3 Advantages of Radio over Fiber

3.3.1 Low attenuation coefficient

Compared to other transmission mediums, optical fiber presents unquestionable lower attenuation coefficient. Today's commercially available fibers can provide attenuations as

low as 0.2dB/km for standard single mode fibers (SMF) in the range of the 1550 nm, or 0.5dB/km in the 1310 nm (the zero dispersion range). Table 3.1 shows the typical attenuation coefficients of usual guided media that is spread around the world in telecommunications systems [23].

Table 3.1 - Transmission characteristics of guided media

	Frequency range	Attenuation	Delay	Repeter spacing
Twisted pair	0 – 1 MHz	3dB/km @ 1 kHz	5μs/km	2 km
Coaxial cable	0 – 500 MHz	7dB/km @ 10 MHz	4μs/km	1 a 9 km
Optical fiber	180 – 370 THz	0.2 to 0.5dB/km	5μs/km	40 km

3.3.2 Large Bandwidth

The utilization of RoF gives use to the enormous bandwidth that fiber can provide. Considering the range of wavelengths for which the attenuation coefficient is bellow 2dB, there are two windows that satisfy this condition. In the range of the 1310 nm wavelength there is a window of 80 nm of bandwidth, and 180 nm in the 1550 nm range.

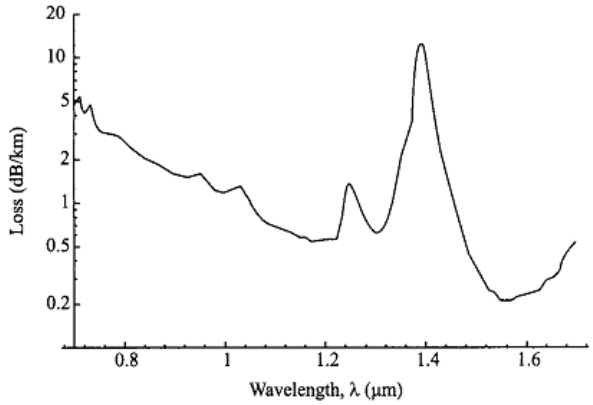

Figure 3.6 - Attenuation loss in silica (After [24])

Such bandwidth, translated in frequency domain, corresponds to about 35000GHz [3]. Such high capacity gives a huge importance to fiber in future telecommunications technologies, since nowadays, only up to 1600GHz are used. There are continuing efforts to benefit more and more from the optical fiber bandwidth. For instance, the use of Optical Time Division Multiplex (OTDM), Dense Wavelength Division Multiplex (DWDM) [25] and Sub-Carrier Multiplex (SCM) [26] [27] [28], which are techniques that combine

several digital signals in only one fiber, distributing them trough time and available bandwidth, can maximize the utilization of bandwidth of the optical fiber.

3.3.3 Immunity to Radio Frequency Interference

Radio over Fiber is within ligthwave technology, which means that signals are transmitted in form of light. It is completely immune to ElectroMagnetic Interference (EMI), like eavesdropping, providing privacy and security, which are also fundamental questions in actual world, where more and more people are dependent on broadband communication systems [22].

3.3.4 Easy Installation and Maintenance

The head scope of the RoF technology is to centralize the complex signal processing at the central office, which therefore will reduce the equipment complexity in the RAUs. In basic RAU systems, only a photodetector, an RF amplifier and an antenna are sufficient to make the RAUs.

Knowing that broadband wireless access needs a high number of RAUs, simpler RAUs will reduce effectively the costs of implementation. Adding to this, simpler and smaller RAUs have smaller failure probability. In cases of failure, maintenance is easier, resulting in many cost savings, taking into account too that some of those RAUs are from difficult access [22].

A possible low-cost system of RoF, from the point of view of the RAUs is presented in [17], which presents a radio-over-fiber downlink based on a silicon avalanche photodetector (APD) fabricated with 0.18- m standard complementary metal–oxide–semiconductor (CMOS) technology. This can be interesting due to the need of implementation of many RAUs.

3.3.5 Reduced Power Consumption

With the concept that RoF technology simplifies all the equipment outside the central office, it is easy to conclude that the power consumption will be smaller. Beyond the system benefits of being easier to fed all the system, it is welcome in a society increasingly concerned in power saving. Researches in Power over Fiber with Radio over Fiber are shown in [29], which brings a new way to feed RAUs without any power grid dependence.

Other perspective is the implementation of passive mode systems, where no power is needed in the RAUs [22].

3.3.6 Dynamic Resource Allocation

In wireless coverage systems, there is the need to control the capacity allocation per cell, since the number of users varies over the day. There are peak times when high concentration of people is in a particular area, such as a soccer stadium, and more capacity needs to be allocated to there in a particular time. The centralization of the services in the central office permits the allocation of optical wavelengths through WDM to provide extra capacity to a RAU, when needed [22]. The central office also can process all the mobility issues, such as handover, easier and quicker [30].

3.4 Impairments in Radio over Fiber

The two most important impairments in RoF links are noise and distortion, the main limitations in analogue links. They affect both the communications between the RAU and the Mobile Unit (MU) (the downlink) and the communications between the MU and the RAU (the uplink). In the downlink, there is the addition of wideband noise, which will increase the interference with other mobiles. In the uplink, the noise link will reduce the RAU sensitivity. The consequence of the distortion is an increase of interference between channels, both for downlink and uplink [12].

These two impairments have very effect in two figures of merit of mobile communication systems, which are the Noise Figure (NF) and the Dynamic Range (DR). The Dynamic Range is related to the different signal powers that may be received by the RAUs, dependent on the distance from the MU and the RAU, since the cell may enclosure an area with radius in the order of magnitude of kilometers.

In the optical link, analogue as well, the noise comes from the laser's Relative Intensity Noise (RIN), laser's phase noise, the photodiode shot noise and the fiber's dispersion. The use of SMF or Multi Mode Fiber (MMF) also has influence in the system's operation. MMF presents much higher dispersion than the SMF, due to modal dispersion.

There is a conventional way to analyze both the previous impairments, which is with the Spur-Free Dynamic Range (SFDR) which is the ratio of the largest to smallest signal that the link can transmit and receive without introducing distortion as shown in. The lower

limit is generally set by noise and the upper limit is by some distortion phenomenon. Distortion occurs from several sources, including second- and third-order harmonics of the signal and the intermodulation distortion (IM) between different channels. The standard technique is to characterize the third-order intermodulation (IM3) products due to two-tone modulation [31].

Figure 3.7 shows how the fundamental signal and IM3 signal vary with input power. The former varies linearly with the input power, and the third-order intermodulation power varies with the cube of the input power. The intersection point of these two curves is known as the third order intercept point [15].

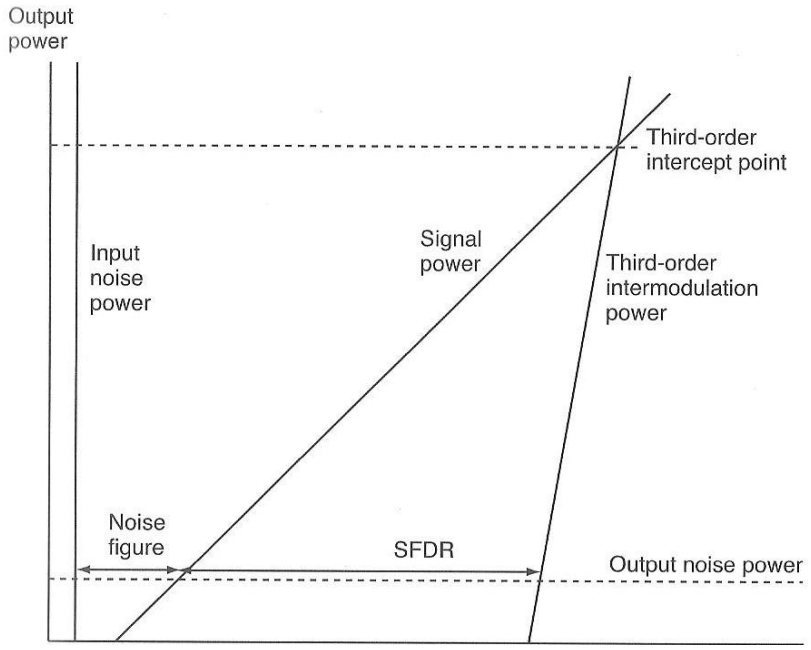

Figure 3.7 - Output power as a function of input power for analog optical links, illustrating system impairments caused by noise and distortion

3.5 Applications of Radio-over-Fiber Technology

Here are discussed main applications where RoF is feasible to be adopted [32].

3.5.1 Cellular Networks

In cellular networks, there is the need to use several antennas to provide full coverage to a certain area. With the increase of mobile users and constant demand on higher capacity, the broadband wireless access providers must have a reliable network to accommodate all the subscribers with a small flaw rate. Here, RoF appears as a good solution, since the antenna's network would keep low costs in maintenance and in

installation, and capacity could be allocated dynamically, due to the centralization of processing functions. Universal Mobile Telecommunications System (UMTS) can benefit from this dynamic allocation, since the area that each antenna can cover reduces with the increase of mobile units.

3.5.2 Satellite Communications

One of the actual implementations of RoF is in the satellite communications. RoF permits to locate all the high frequency equipment apart from the antenna site using the fiber characteristics (high bandwidth, low losses,…) to convey the microwave signals. The remote positioning of the antennas can be viewed in a small scale, the antennas are within the satellite earth stations and small length fiber is needed; or in a high scale, positioning the antennas kms away from the satellite earth station, where the signal transmission and reception may be improved due to atmospheric conditions.

3.5.3 Video Distribution Systems

One of the many application areas of RoF systems is video distribution. In particular, the Multipoint Video Distribution Services (MVDS), which is a cellular terrestrial transmission system for video broadcast. Allocated frequencies for this service are in the 40 GHz band. At these frequencies, the maximum cell size is about 5km. The RoF system can have a good implementation since the processing units can be located in one place only and the antennas can be upgraded easily if the more services are added and capacity is required.

3.5.4 Mobile Broadband Services

The Mobile Broadband System or Service (MBS) concept is intended to extend the services available in fixed Broadband Integrated Services Digital Network (B-ISDN) to mobile users of all kinds. This system operates in the range of 62-66GHz, to be able to provide the 155Mbps to each user. In those frequencies, the cell area is very small (pico-cells), requiring therefore many antennas to cover the desired area. RoF is once more a good application here, due to its high bandwidth, not to mention the cost benefits.

3.5.5 Wireless LANs

Nowadays, Internet wireless access is fully emerging as a ubiquity service. People are massively dependent on Internet access, and wireless access provides freedom and

comfort. Once more, this huge adoption in people lives brings the need of having even better service. This requires an upgrade in capacity of the network. For instance current wireless LANs operate at the 2.4 GHz industrial, scientific and medical (ISM) bands and offer the maximum capacity of 11 Mbps per carrier. Next generation broadband wireless LANs are primed to offer up to 54 Mbps per carrier, and will require higher carrier frequencies in the 5 GHz band.

Higher carrier frequencies will demand smaller cells, which is traduced in implementations with numerous antennas. Using the benefits of RoF, the deployment of the wireless network can be followed by a low cost infrastructure and have a central office with all the information updated.

3.5.6 Vehicle Communication and Control

The objective is to provide continuous mobile communication coverage on major roads for the purpose of Intelligent Transport Systems (ITS) such as Road-to-Vehicle Communication (RVC) and Inter-Vehicle Communication (IVC). Its objective is to exchange traffic information and achieve safe and comfortable driving [20]. Frequencies between 63-64 GHz and 76-77 GHz have already been allocated for this service within Europe. To implement this system, there are needed several antenna sites, to cover the road length. Therefore, RoF can be a good system to deploy this technology.

3.6 Analog Optical Links

Radio over Fiber is an analog transmission system, since it distributes the signal directly at the radio carrier frequency, from the CO to the RAU/BS. This is the main difference from the most widely spread optical fiber transmitting systems. There are three approaches to transport radio signals in RoF systems, which are classified based on the frequency bands used: RF signal, intermediate frequency (IF) signal and baseband (BB) signal, as shown in Figure 3.8.

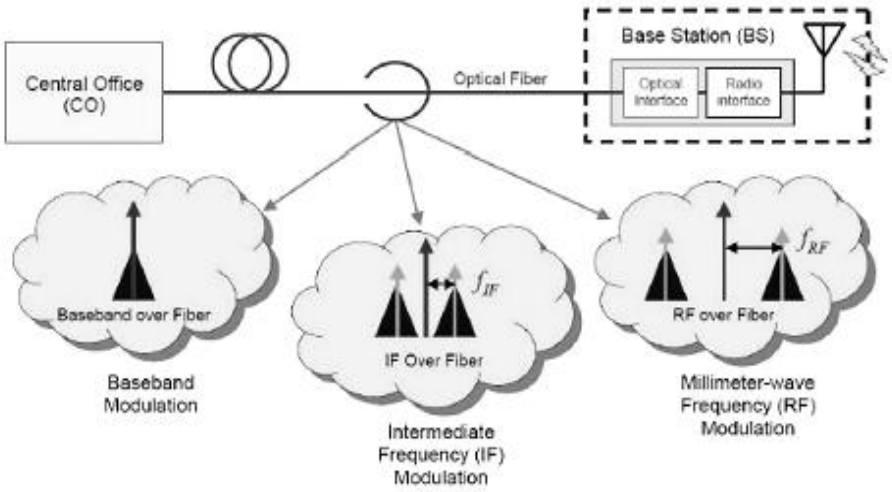

Figure 3.8 - Radio signal transport schemes for RoF systems

The signal can be modeled into optical waveform through direct or external modulation. RoF is probably the most straightforward radio signal distribution technology because the wireless signals are transported directly over the fiber at the radio carrier transmission frequency without the need for any subsequent frequency up or down conversion at the RAU/BS. Ideally, the output signal from the optical link will be a copy of the input radio signal.

3.6.1 Radio Signal Generation

In RoF systems, the optical signal is generated by intensity modulation (IM). There are three methods for generate optical signal by intensity modulation:

a) Direct Modulation;

b) External Modulation;

c) Remote Heterodyning.

In the first method, the RF signal is the electrical source of the laser, hence the name. In the second method, the optical modulation is performed by an external modulator. The laser provides a CW optical beam, and then an external modulator such as the MZM, modulates the intensity of the light. In the third method, RF signals are optically generated via remote heterodyning, that is, a method in which more than one optical signal is generated by the light source, one of which is modulated by the information-bearing signal

and these are mixed or heterodyned by the photodetector or by an external mixer to form the output RF signal. Only direct and external modulation will be analyzed in this text.

3.6.2 Direct Modulation

Direct modulation is the simplest and the cheapest of the three possible solutions, since no other components are required for modulation other than the light source itself. Therefore, efforts are constantly made to apply it anywhere possible. A direct-modulation link is so named because a semiconductor laser directly converts a small-signal modulation (around a bias point set by a dc current) into a corresponding small-signal modulation of the intensity of photons emitted (around the average intensity at the bias point). Thus, a single device serves as both the optical source and the RF/optical modulator [33]. An IM-DD optical link is shown in Figure 3.1.

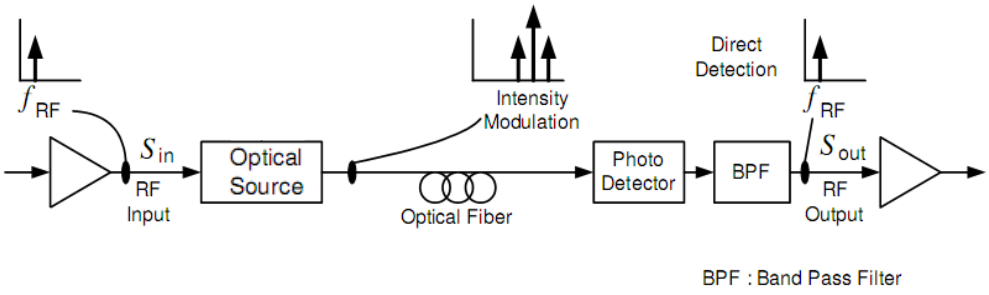

Figure 3.9 - Definition of an intensity-modulation direct-detection (IM-DD) analog optical link.

A major advantage of semiconductor lasers is that they can be directly modulated. In contrast, many other lasers are continuous wave sources and cannot be modulated directly at all, needing an external modulator.

Lasers suffer from chirp, RIN and non-linear distortion, which will be main degradation factors in directly modulated links. Other disadvantage of direct modulation is the laser's bandwidth. Simple lasers can be modulated up to 5-10GHz. Above theses frequencies, external modulation is applied instead. In entering into the millimeter band a new adverse effect, such as the nonconvenient transfer function of the transmission medium, is observed. It turns out that the fiber dispersion and coherent mixing of the sidebands of modulated light may cause transmission zeros, even in the case of rather moderate lengths of fiber. For instance, a standard fiber having a one km length has a transmission zero at 60 GHz if 1.55 μm wavelength light is intensity modulated [20].

RoF systems require a high carrier-to-noise ratio (CNR), and CNR can be strongly influenced by the RIN of the source laser. A study have shown substantial CNR degradation at higher frequencies, which increases with fiber chromatic dispersion and laser linewidth. Analog lasers should be chosen on the basis of both RIN and linewidth performance [34].

3.6.3 External Modulation

It is usual to use a MZM in external modulation configurations. Its wider modulation bandwidth, higher performance and RIN reduction, compared with direct modulation; such a modulator provides functions such as modulation, harmonic-generation, and electro-optical up-conversion. External modulation is, in contrast, more expensive than direct modulation, since the intensity modulation is carried by an external modulator, which is usually expensive.

Due to the inherent nonlinearity of MZM, larger input signal level means larger nonlinear distortion. The intermodulation terms severely degrade the system performance because the power of intermodulation is higher than the noise power for high input powers. Third-order intermodulation (IM3) terms are very important since and their powers increase faster than the fundamental and limit the dynamic range of the system [35] as seen in Figure 3.7.

Figure 3.10 shows an IM-DD optical link using a RF/Optical Modulator different from the optical source.

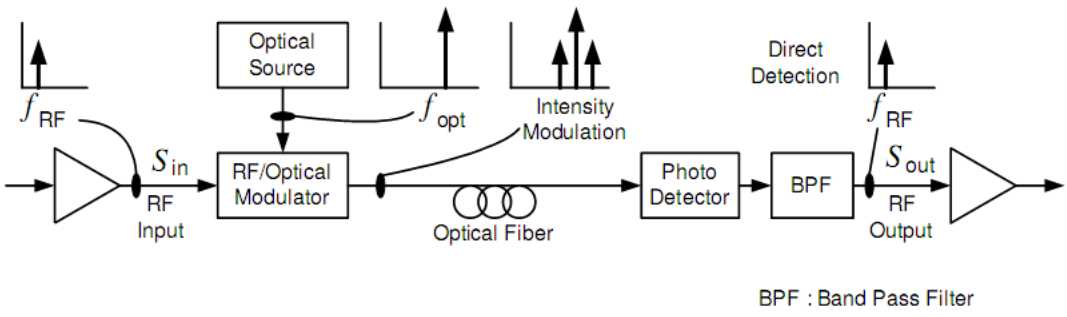

Figure 3.10 – IM-DD analog optical link with external modulation

As we can see, the optical source only produces the optical carrier. The external modulator will therefore use the RF signal to apply the intensity modulation. This way the

lasers RIN is reduced as well as the chirp. Albeit the external modulator is expensive, there have been conducted several studies in RoF systems [36-39].

4

Simulation of a RoF-WLAN System

4.1 Introduction

This chapter presents the results of the analysis conducted to test the power estimation coefficient efficiency and its effects in the EVM evaluation. It presents either two RoF-WLAN systems developed in the OSIP software. The first is an optical setup with external modulation method, and in the second apply direct modulation. Both simulation results are compared to experimental and VPI© simulation results.

4.2 Power Estimation an EVM Evaluation of QAM Finite Sequences

To demonstrate the power estimation coefficient method efficiency derived in section 2.2.4, it has been used an optical setup in external modulation configuration. It is presented in the Figure 4.1:

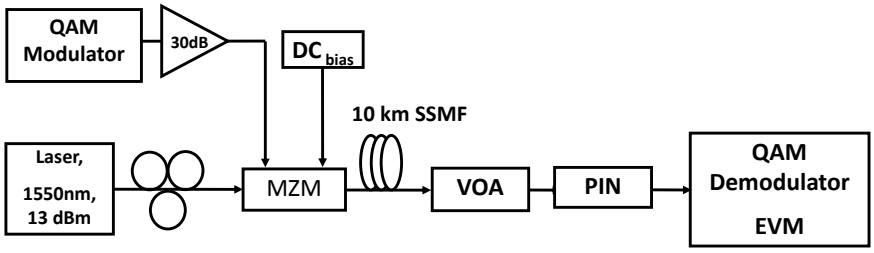

Figure 4.1 - External modulation setup. MZM – Mach Zehnder Modulator; VOA – Variable Output Attenuator; PIN – *p-i-n* Photodiode; SSMF – Standard Single Mode Fiber.

The EVM evaluation (eq (2.68)) of the first simulations has resulted in values which were inaccurate (the value was varying significantly from simulation to simulation) and not precise (the estimative variance was very large). It has been found out that this lack of precision was due to the received signal power estimation. Therefore, a new method [40] is proposed to improve the estimation of the QAM mean signal power.

The new method is introduced in section 2.2.4 and presents a correction factor S_x (eq (2.66)) for the power estimator. It was applied in the QAM Demodulator of the setup presented in the Figure 4.1. In order to understand the optimization made by the correction factor (S_x), we have made 50 simulations of four different values for the symbol sequence length (10, 50, 100 and 150 symbols). The results are presented in Table 4.1 and Table 4.2, respectively for power estimation and EVM evaluation without and with correction factor S_x.

Table 4.1 – Correction factor (S_x) effect on the power estimation.

	Sequence length (symbols/bits)	Mean (dBm)	Standard Deviation (dBm)
With S_x	10/60	-62.08	0.015
	50/300	-62.08	0.005
	100/600	-62.08	0.005
	150/900	-62.08	0.003
Without S_x	10/60	-62.18	0.89
	50/300	-62.20	0.40
	100/600	-62.08	0.28
	150/900	-62.13	0.21

Table 4.2 - Correction factor (S_x) effect on the EVM evaluation

	Sequence length (symbols/bits)	Mean (%)	Standard Deviation (%)
With S_x	10/60	1.16	0.18
	50/300	1.15	0.08
	100/600	1.16	0.06
	150/900	1.17	0.05
Without S_x	10/60	6.16	4.03
	50/300	2.76	1.70
	100/600	2.12	1.09
	150/900	1.80	0.74

Confronting results in both Table 4.1 and Table 4.2, it is possible to recognize the effectiveness of the correction factor. Both precision and accuracy have improved, and the power estimation became practically independent of the sequence length. It is remarkable that using S_x and a 10 symbol length sequence, the results are more accurate and precise than without using S_x in a 150 symbol sequence. This outcome is specifically advantageous in simulating systems, were the simulation time does not increase linearly with the sequence length, but in a higher degree.

4.3 External Modulation Setup

The external modulation setup used in the study of this scenario is shown in the Figure 4.2. The radio signal scheme is the intermediate frequency (IF) modulation, since the electrical carrier frequency is 1GHz, instead of the 2.4GHz defined by the WiFi standard. However, the conversion between the intermediate to the radio frequency is obtained with local oscillators in the transmitter as well as in the receiver.

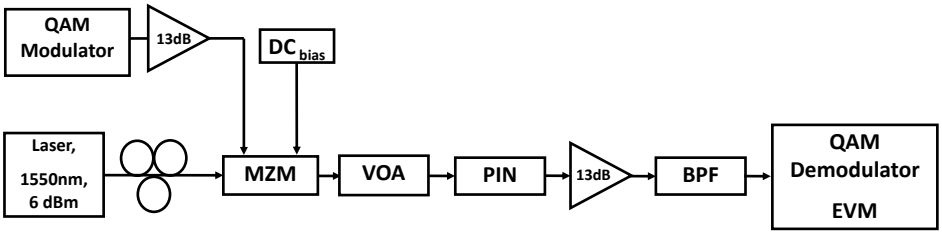

Figure 4.2 – External modulation setup; BFF – Bandpass Filter.

The results presented from experimental setup, as well as from the VPI© simulation, were provided by one of the partners of the FUTON project.

To emulate optical losses, such as fiber losses and coupling, a Variable Optical Attenuator VOA was set with an attenuation factor of 3.8dB. The noise sources used in photodiode *p-i-n* where the shot and the thermal noise, this latter of $15\,pA/\sqrt{Hz}$. The responsivity of the photodiode was 0.75A/W.

It was used a low pass equivalent to transmit the optical power in the baseband, in order to decrease the computational requirements. To sample de signal it was used a 10GHz sampling frequency.

4.3.1 Laser

The laser produce a CW output with 6dBm average optical power. The center wavelength is 1550nm. The Figure 4.3 shows the laser's output optical spectrum. The linewidth of the laser is 10MHz.

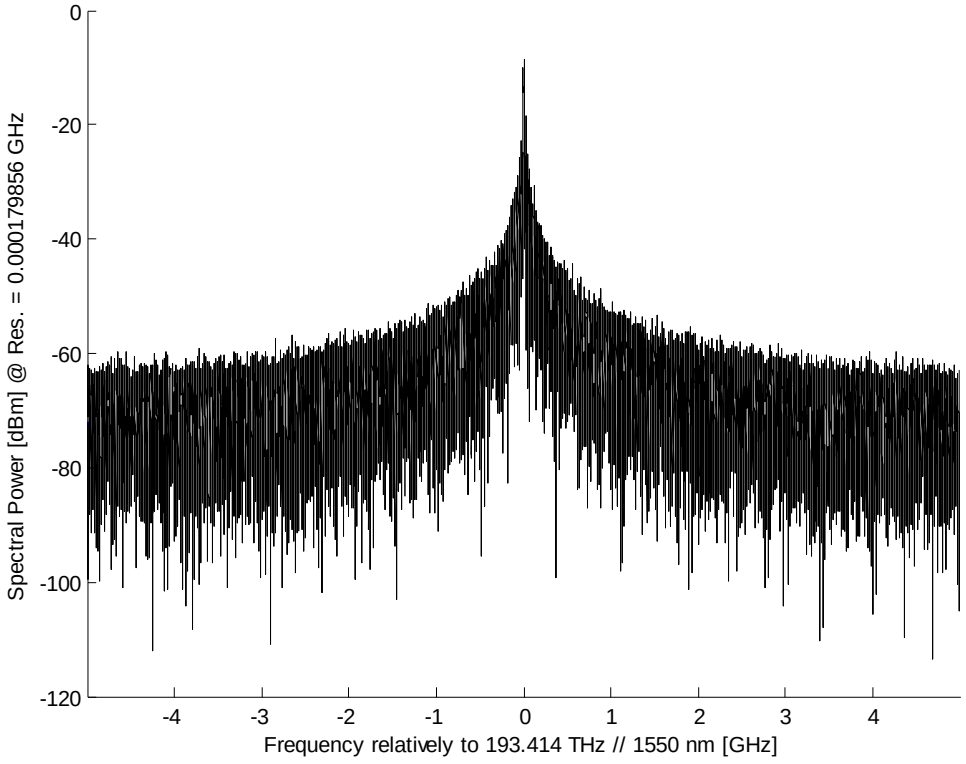

Figure 4.3 - Output Continuous Wave (CW) laser optical spectrum.

4.3.2 QAM Modulator

The QAM modulator produces an M-QAM electric signal output, with a user-specified average power, symbol length and number of constellation symbols, M. The output of the QAM modulator is shown in Figure 4.4. It follows the modulation referred in

eq (2.61) and it is possible to denote the amplitude and the phase modulation as the symbol changes to the next one. The carrier frequency used was w_c=1GHz and the number of bits coded into each symbol were 6, thus M=2^6.

The output waveform present in the Figure 4.4 is generated taking into account that the average power specified refers to 1Ω impedance.

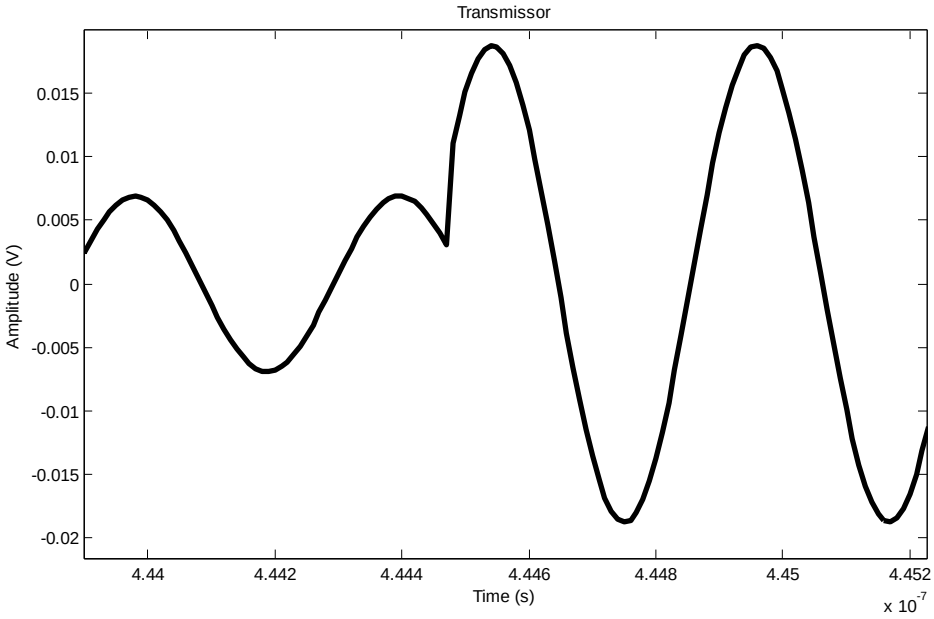

Figure 4.4 - QAM signal wavelength, denoting the moment when the symbol changes.

The signal spectrum is show in Figure 4.5.

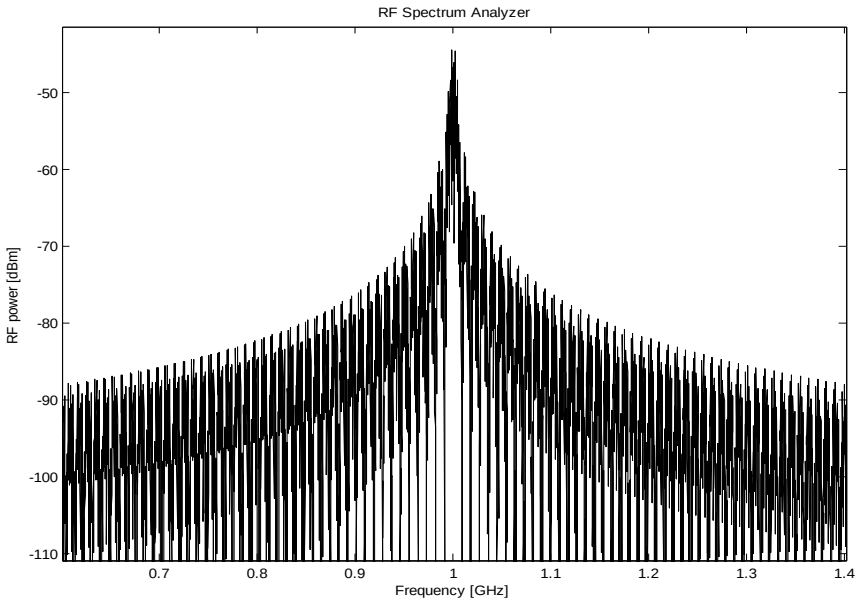

Figure 4.5 - QAM signal spectrum.

The MZM was configured in the push-pull operation, as shown in Figure 2.11, and was set with $V_\pi = 5.5V$ and insertion losses IL=4.1dB. Figure 4.6 presents the transfer function P_{MZM_out} / P_{MZM_in} versus $V_M = v_1(t) - v_2(t)$, which is the differential voltage between the two electrodes in the MZM push-pull configuration shown in Figure 2.11.

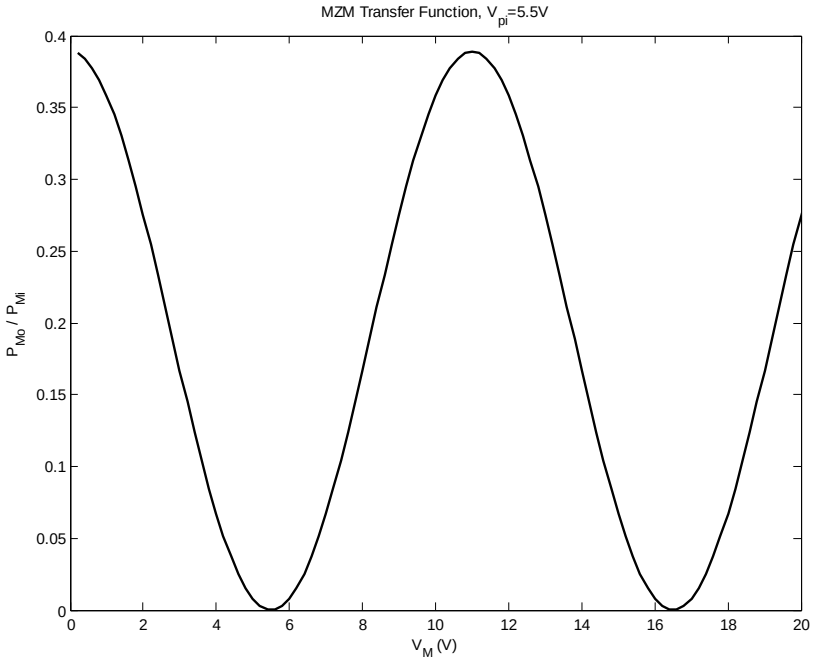

Figure 4.6 - MZM transfer function. P_{Mo} and P_{Mi} are the optical power at the output and at the input of the modulator, respectively. V_M is the differential voltage between drive electrodes in the MZM push-pull configuration.

As one can see, the transfer function in Figure 4.6 is not linear. It depends largely on the bias voltage V_M (eq (2.48)). If V_M=V_π the optical waves traveling in both arms cancel each other in the coupler due to phase opposition, as seen in section 2.1.4. The most linear response of the MZM is with $V_M = \frac{V_\pi}{2}$ (inflexion point of its transfer function, see Figure 4.6), for small-signal models.

Due to its nonlinear transfer function, the modulating signal cannot be as high as one wants. The intermodulation products have high influence on the link, and they can be seen in Figure 4.7. At 2GHz appear components that result from the beats between the IF signal and the optical carrier.

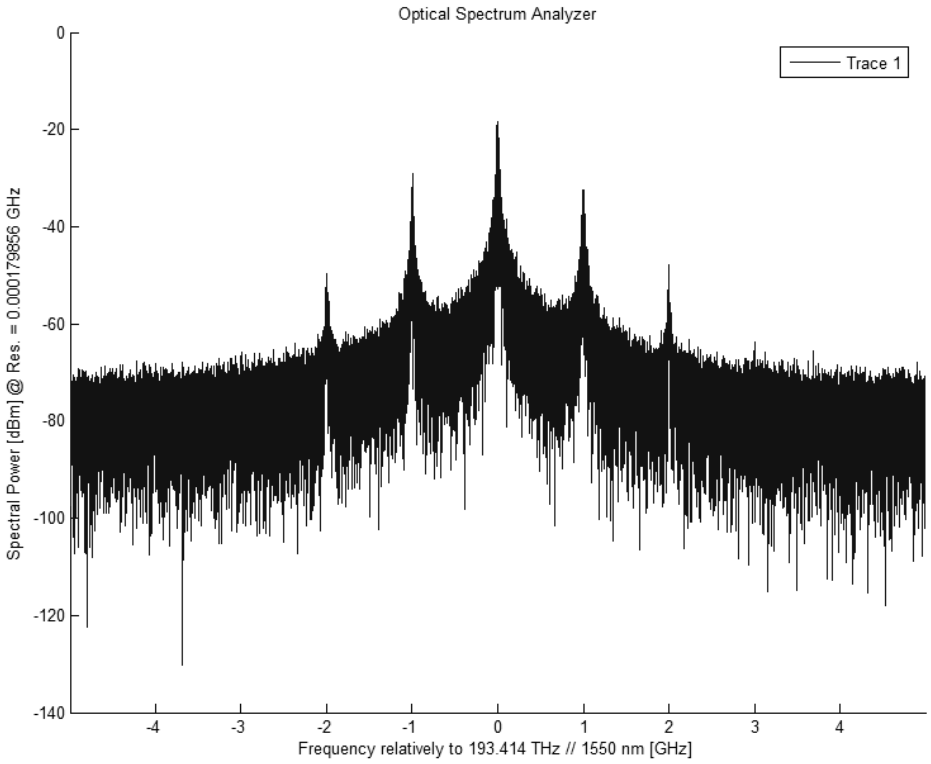

Figure 4.7 – Optical Spectrum after MZM, for 8*dBm* input electrical signal power.

The QAM demodulator and EVM evaluator follow the schematic shown in Figure 2.16.

4.3.3 Link Gain

Here, it is derived the small-signal relation between the drive voltage of the MZM and the photocurrent generated in the photodiode to obtain the link gain of the externally modulated link.

The MZM is configured in push-pull configuration and its transfer function is given by:

$$\frac{E_{MZM\_out}(t)}{E_{MZM\_in}(t)} = \frac{1}{2A_{tt}}\left(e^{j\left(\frac{\pi}{V_\pi}v_{RF}(t)-\frac{V_\pi}{4}\right)} + e^{-j\left(\frac{\pi}{V_\pi}v_{RF}(t)-\frac{V_\pi}{4}\right)} \right) \tag{4.1}$$

From the well known trigonometric identity $\cos(x) = \frac{e^{jx}+e^{-jx}}{2}$,

$$\frac{E_{MZM\_out}(t)}{E_{MZM\_in}(t)} = \frac{1}{A_{tt}}\cos\left(\frac{\pi}{V_\pi}v_{RF}(t)-\frac{\pi}{4}\right)$$

$$= \frac{1}{A_{tt}} \cos\left(\frac{\pi}{V_\pi} v_{RF}(t)\right) \cos\left(\frac{\pi}{4}\right) + \sin\left(\frac{\pi}{V_\pi} v_{RF}(t)\right) \sin\left(\frac{\pi}{4}\right)$$

$$= \frac{1}{A_{tt}} \left(\frac{\sqrt{2}}{2} \cos\left(\frac{\pi}{V_\pi} v_{RF}(t)\right) + \frac{\sqrt{2}}{2} \sin\left(\frac{\pi}{V_\pi} v_{RF}(t)\right) \right) \quad (4.2)$$

When considering small-signal model, it is possible to approximate the MZM highly nonlinear transfer function to a first order function, by the Taylor theorem. It states that the linear approximation of the differentiable function $y = f(x)$, around x_0, is given by:

$$y = f(x_0) + (x - x_0) f'(x_0) \quad (4.3)$$

$$f'(x_0) = \left.\frac{\partial y}{\partial x}\right|_{x=x_0} \quad (4.4)$$

The MZM is generally biased at one of the inflexion points of the transfer function presented in Figure 4.6. It will be considered here the point given by $V_M = \frac{3V_\pi}{2}$, which corresponds therefore to x_0.

Considering $y = \frac{E_{MZM\_out}(t)}{E_{MZM\_in}(t)} = f\left(v_{RF}(t)\right)$,

$$f'\left(v_{RF}(t) = \frac{V_\pi}{2}\right) = -\frac{\sqrt{2}\pi}{2V_\pi A_{tt}} \sin\left(\frac{\pi}{V_\pi} v_{RF}(t)\right) + \frac{\sqrt{2}\pi}{2V_\pi A_{tt}} \cos\left(\frac{\pi}{V_\pi} v_{RF}(t)\right)\Bigg|_{v_{RF}(t)=\frac{3V_\pi}{2}} \quad (4.5)$$

$$= -\frac{\sqrt{2}\pi}{2V_\pi A_{tt}} \quad (4.6)$$

$$f\left(v_{RF}(t) = \frac{V_\pi}{2}\right) = \frac{\sqrt{2}}{2A_{tt}} \quad (4.7)$$

The small-signal model of the MZM is, therefore, given by:

$$\frac{E_{MZM\_out}(t)}{E_{MZM\_in}(t)} = \frac{\sqrt{2}}{2A_{tt}} + \frac{\sqrt{2}\pi}{2V_\pi A_{tt}} v_{RF}(t) \quad (4.8)$$

The electric field incident, $E_{MZM\_in}(t)$, is generated by the CW laser at the w_o optical carrier frequency:

$$E_{CW}(t) = A_o \cos(w_o t) \tag{4.9}$$

The VOA is used to emulate optical losses, like fiber and coupling. It is defined by an attenuation of $10dB$, and the electric field at the photodiode is then:

$$E_{pin}(t) = \frac{1}{A_{VOA}}\left(\frac{\sqrt{2}}{2A_{tt}} + \frac{\sqrt{2}\pi}{2V_\pi A_{tt}} v_{RF}(t)\right) E_{CW}(t) \tag{4.10}$$

$$= \left(\frac{\sqrt{2}}{2A_{tt}A_{VOA}} + \frac{\sqrt{2}\pi}{2V_\pi A_{tt}A_{VOA}} v_{RF}(t)\right) A_o \cos(w_o t) \tag{4.11}$$

The photodiode is a transducer, which converts a beam of photon into electrons, generating the photocurrent, and the relation between these quantities is given by eq.(2.45). The optical power incident to the photodiode is given by[1]:

$$I_{pin} = RP_{pin} \tag{4.12}$$

$$= R\left\langle E_{pin}E_{pin}^{*}\right\rangle \tag{4.13}$$

$$= R\left[\left(\frac{\sqrt{2}}{2A_{tt}A_{VOA}} + \frac{\sqrt{2}\pi}{2V_\pi A_{tt}A_{VOA}} v_{RF}(t)\right) A_o \cos(w_o t)\right]^2 \tag{4.14}$$

$$= R\left[\frac{A_o^2}{2A_{tt}^2A_{VOA}^2}\cos^2(w_o t) + \frac{\pi A_o^2}{V_\pi A_{tt}^2 A_{VOA}^2} v_{RF}(t)\cos^2(w_o t) + \right.$$

$$\left. + \frac{\pi^2 A_o^2}{2V_\pi^2 A_{tt}^2 A_{VOA}^2} v_{RF}^2(t)\cos^2(w_o t)\right] \tag{4.15}$$

The trigonometric simplification $\cos^2(x) = \frac{1}{2} + \frac{1}{2}\cos(2x)$ can be used, as well as the knowing that the photodiode is an envelope detector, hence the frequency terms disappear.

[1] $\langle x \rangle$ represents the mean of x.

Also, another simplification can be made, $\pi v_{RF}(t) \ll V_{\pi}$, since small-signal modeling is applied.

Hence the photocurrent is given by:

$$I_{pin} = R\left[\frac{A_o^2}{4A_{tt}^2 A_{VOA}^2} + \frac{\pi A_o^2}{2V_{\pi} A_{tt}^2 A_{VOA}^2} v_{RF}(t)\right] \tag{4.16}$$

And the small signal photocurrent is:

$$i_{pin}(t) = \frac{R\pi A_o^2}{2V_{\pi} A_{tt}^2 A_{VOA}^2} v_{RF}(t) \tag{4.17}$$

The externally modulated link gain is given then by:

$$G_{em} = \frac{i_{pin}(t)}{v_{RF}(t)} = \frac{R\pi A_o^2}{2V_{\pi} A_{tt}^2 A_{VOA}} \tag{4.18}$$

In Table 4.3 one can compare the calculated link gain from the eq. (4.18) and the link gain obtained from simulation with OSIP.

Table 4.3 - Externally modulated link gain calculated and simulated.

Link Gain obtained with the eq. (4.18)	OSIP
$2,764 * 10^{-4}$	$2,767 * 10^{-4}$

The link gain from the approximation derived is close to the OSIP link gain result. The approximation is therefore correct.

4.3.4 Externally Modulated Link Performance

Figure 4.8 is a comparison of measured and simulated EVM for an 802.11g signal with the external modulation setup.

From the obtained results, it is seeable that the possible input power range is limited to 25-30dB, considering that the EVM limit is defined as 5.6% [41]. There are two distinct impairments that define those limits.

In the upper limit, the nonlinearities of the MZM transfer function are responsible for the fast increasing of the EVM values. In this range, both simulation programs have values slightly apart from the experimental. If the modulator transfer function is not as perfect as the one presented in the Figure 4.6, and with high electrical input power, it may have a different behavior, resulting in the discrepancy between simulation and experimental results.

In the lower limit, noise from the detector is the fundamental impairment to the signal transmission. There are two fundamental noise sources from the photodiode: the shot and the thermal noise. The OSIP results in this range are close to the experimental data (less than 0.7% difference), however do not present a complete match. This difference may be due to the noiseless electrical signals treatment in this work, or related to the electrical signals coupling in the MZM arms.

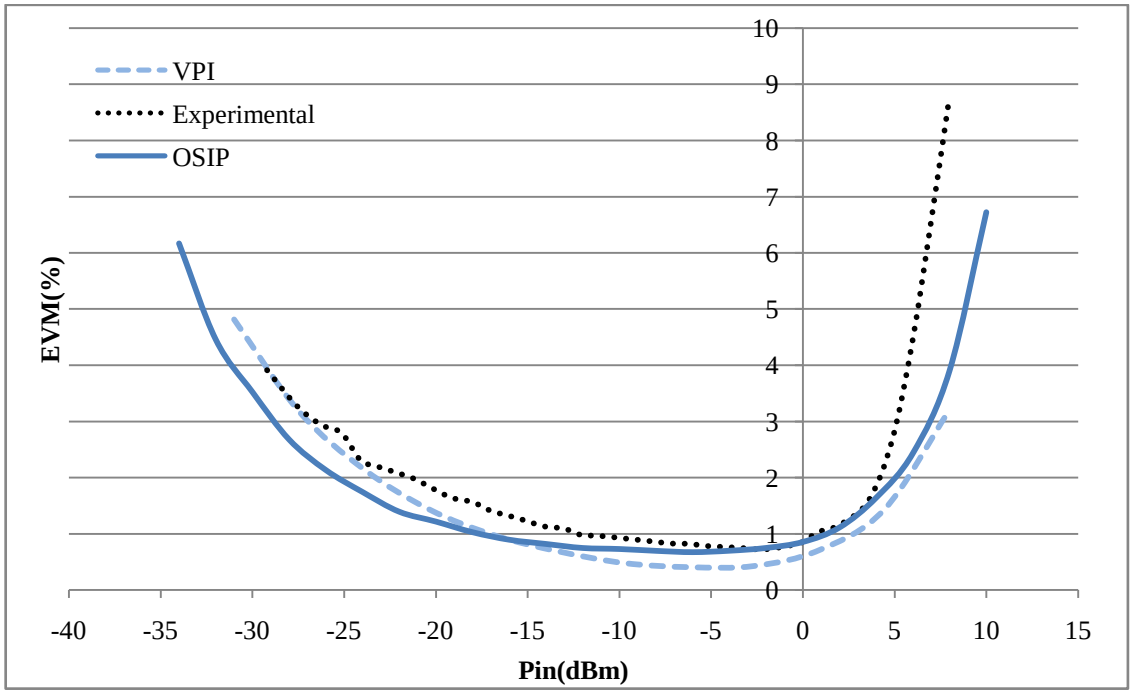

Figure 4.8 – EVM vs Input Power comparison between VPI©, OSIP and experimental results for externally modulated link. Input power referees to input electrical power in the MZM.

4.4 Direct Modulation Setup

The direct modulation scenario (Figure 4.9) is the simplest approach in RoF, but has several impairments that contribute to the degradation of the transmitted signal, mainly from the laser (chirp, RIN, and non-linear distortion).

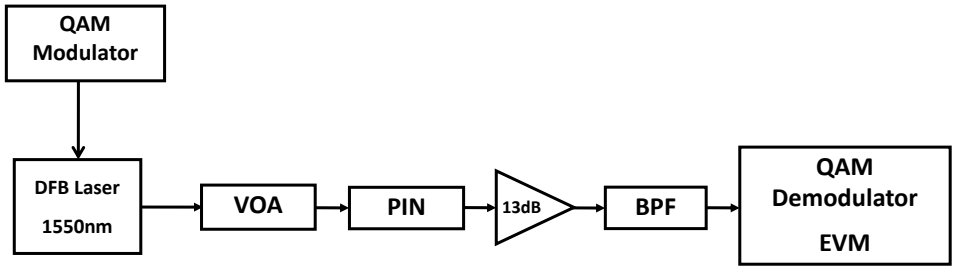

Figure 4.9 - Direct modulation setup; BPF - bandpass filter.

To emulate optical losses, such as fiber losses and coupling, a Variable Optical Attenuator VOA was set with an attenuation factor of 10dB. The noise sources used in photodiode *p-i-n* where the shot and the thermal noise, this latter of $10\,pA/\sqrt{Hz}$. The responsivity of the photo diode was 1A/W.

4.4.1 Laser

The laser used in the setup of the Figure 4.9 is a DFB laser developed specifically to the FUTON project, optimized for RoF specifications, and its parameters are presented in the Table 4.4.

Table 4.4 – Parameters used in OSIP and VPI.

Emission Frequency (*Hz/nm*)	f_o/λ_o	193.1e12/1550
Differential Gain (m^3/s)	g_o	1.71e-11
Transparency Carrier Density ($1/m^3$)	n_o	5.4e24
Carrier Lifetime (*s*)	τ_n	1.32e-9
Photon Lifetime (*s*)	τ_p	1.6e-12
Optical Confinement Factor	Γ	0.1
Non-linear Gain Compression Factor (m^3)	ε	5e-23
Spontaneous Emission Factor	β_s	1e-4
Active Volume (m^3)	V	4.14e-17
Optical coupling efficiency	η	0.03
Linewidth Enhancement Factor	α_H	4

From (2.38) one can obtain the amplitude response of the laser with the parameters from Table 4.4. The Figure 4.10 presents the amplitude response for four bias current values I_o: 75, 100, 125 and 150mA. In Figure 4.11 is shown the frequency and phase response of the DFB laser, for the same bias current values.

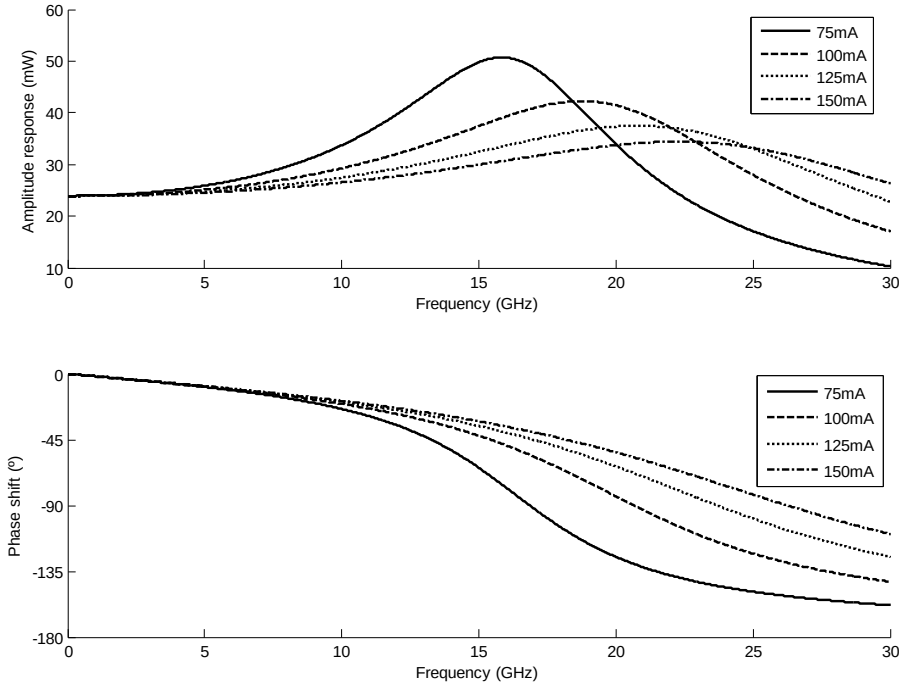

Figure 4.10 - Amplitude and phase response of the DFB laser

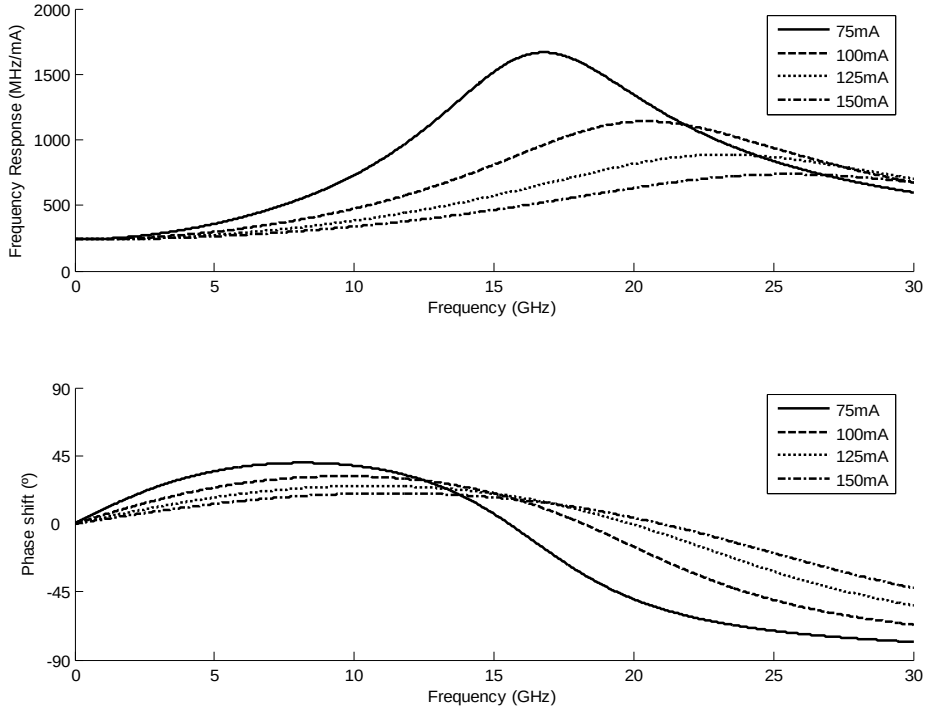

Figure 4.11 - Frequency and phase response of the DFB laser

Figure 4.10 and Figure 4.11 show that the resonance frequency of the laser depends on the bias current. It is approximately 16GHz for 75mA, and approximately 25GHz using a bias current equal to 150mA. This is appropriate for RoF, since it brings the laser nonlinearities near the resonance frequency range distant from the RF operating frequency. Also the amplitude has a flattener response for the latter bias current.

The chirp of this laser is approximately 250MHz/mA.

The static P-I characteristic of the DFB laser mentioned is presented in the Figure 4.12. As it is clearly observed, the experimental curve is not linear. The OSIP model does not take into account this factor, and therefore, presents some different from the experimental setup. The VPI© curve was modeled only with the threshold current and the slope efficiency measured from experimental values.

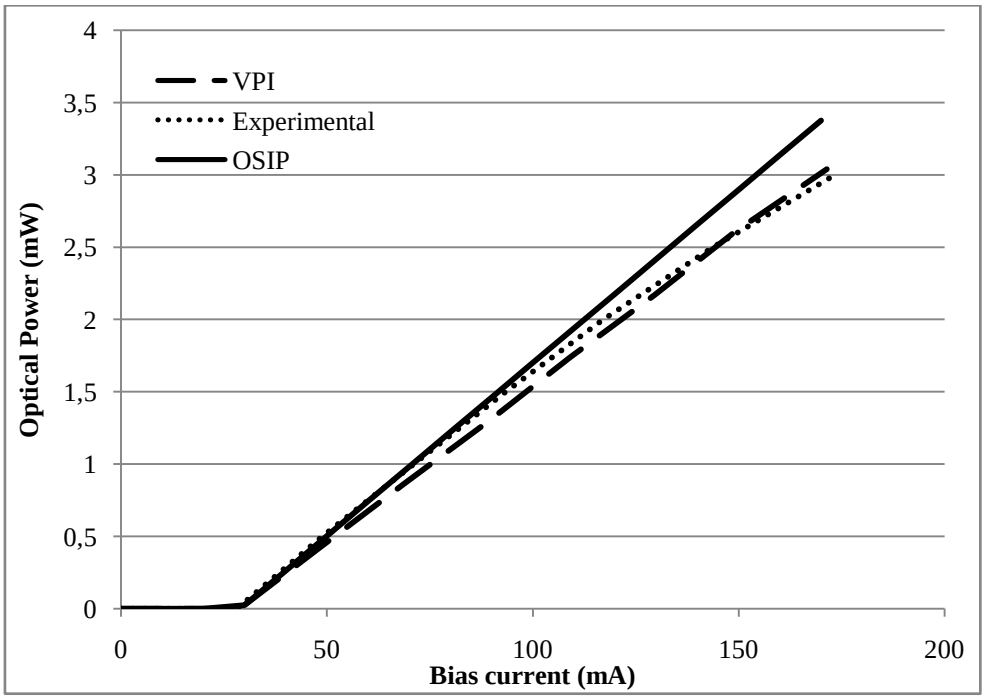

Figure 4.12 – Modeled static characteristic (P-I curve), with I_{th}=29mA.

4.4.2 Link Gain

The directly modulated link gain can be found by [42]:

$$G_{dm} = \left(\frac{\eta R}{L_{opt}} \right)^2 \tag{4.19}$$

where η is the efficiency of the laser, R is the responsivity of the photodiode, and L_{opt} is the losses in the optical link. In the Table 4.5, it is compared the link gain with ideal and with real coupling efficiency.

Table 4.5 - Directly modulated gain link from eq. (4.19), for the modeled and the measured coupling efficiency.

Modeled (η=0.03W/A)	**Measured (η=0.022W/A)**
$2.85 * 10^{-4}$	$1.53 * 10^{-4}$

From the presented results, it is possible to verify the influence of the optical coupling efficiency in the link gain for the directly modulated link. With a decrease of the coupling efficiency of 0.008W/A, which is 27% of the ideal value, the link gain decreased in 46%.

4.4.3 Directly Modulated Link Performance

Figure 4.13 is a comparison of measured and simulated EVM for an 802.11g signal with the direct modulation setup presented in Figure 4.9. The results presented from experimental setup, as well as from the VPI© simulation, were provided by one of the partners of the FUTON project.

The laser model required a sampling frequency of at least 300GHz to provide acceptable results.

At the first glance, it is possible to observe two distinct differences between the results. First, the EVM lower limit in OSIP results is approximately 0.9% larger than the experimental results at 0dBm input power. Also the OSIP results reach the lower limit (≈1.9%) at -15dBm of input power, whereas the experimental, as well as VPI© results decrease until 0dBm of input power. A possible cause is the laser's RIN, which could be different from VPI© and experimental results. However, it was not possible to know the experimental or the VPI© modeled laser's RIN value.

The other difference mentioned above is related to the low input power results, where the impairments are predominantly affected by the receiver noise. From -15dBm to -26 dBm, despite the results diverge from the experimental, it matches the VPI© results. However, at powers lower than -26dBm, the OSIP performance degrades in a higher

degree than the VPI© or experimental setup: at -35dBm of input power, the discrepancy between OSIP to experimental results is approximately 5%, and 6% if we refer to VPI© simulations. The divergence of those values possibly was related with the fact that the experimental and the VPI© thermal noise values were unknown. The modeled thermal noise in OSIP could be overvalued and then the mismatch of the curves.

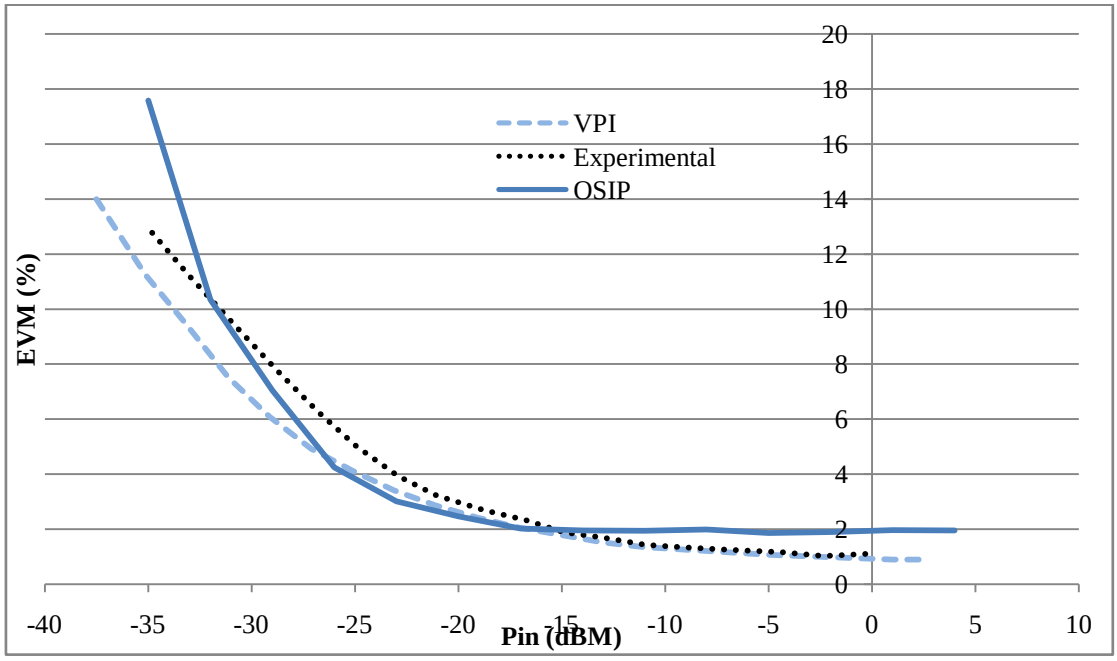

Figure 4.13 - EVM vs Input Power comparison between VPI©, OSIP and experimental results for directly modulated link. Input power referees to input electrical power in the DFB laser.

5

Conclusions, Future Work

In this final chapter are presented some general conclusions about the work developed and also some topics that may be exploited in future research and developments.

5.1 Conclusions

Throughout this work it was developed and implemented some models required to enable the simulations of Radio-over-Fiber systems in the OSIP software. The results obtained were compared to experimental measurements, and also with other simulating software, the VPI©.

In order to make possible the required simulations, it was derived a correction factor for power estimation, which allowed to nearly eliminate the dependence of the power estimation on the QAM sequence length. It was submitted and accepted the following paper [40] to SEON's – Symposium of Enabling Optical Networks and Sensors, which

presents the effect of the correction factor in the received power and further in the EVM evaluation:

H. L. Moura, Paulo P. Monteiro, Rui S. Ribeiro, "Power Estimation and EVM Evaluation of QAM Finite Sequences," *SEON's,* 2009.

Two different Radio-over-Fiber scenarios were implemented: direct and external modulation setups. In external modulation, it was derived the link gain and compared to the simulations result. It also has been compared the performance, in terms of EVM, of the implemented models in OSIP with VPI© and with measured data from laboratory experiments.

In direct modulation, it have been included the DFB laser model, which solves the nonlinear rate equations, and was adapted from SCORE, another simulating software in optics field, developed by professor Rui Sousa Ribeiro, PhD. Due to the severe computational requirements with this model, once more, the correction factor was crucial to permit the simulations of the system. As with external modulation, it was presented the comparison between results obtained from OSIP, VPI© and the laboratory measurements.

5.2 Future Work

It is important to improve the direct modulation modeling, namely the study of the constraints that inhibit the complete match of the simulated with the measured results.

From the work developed, one future topic would be an extensive analysis of the electrical noise in both RoF scenarios. It would improve the performance of the models implemented, from the fact that Noise Figure is a figure of merit in RoF systems.

It is also important, since this is optics, to introduce the effect of the fiber in both externally or directly modulated links. The chirp of the DFB laser, together with the chromatic desertion may cause severe distortion in the modulated signal.

Implementing other standards existent today, with different electrical carrier frequencies, baud rates, and modulation formats should be interesting to analyze the effect of conveying multi-standard signals with SCM through RoF systems.

Finally, it can be modeled and analyzed a Distributed Antenna System that would give the perspective of implement RoF as a low-cost system in public places, like hospitals, shopping malls, etc.

References

[1] G. Keiser, *Opical fiber communications*, 2nd ed. New York, 2000.

[2] G. P. Agrawal, *Fiber-optic communication systems*, 3rd ed. New York, 2002.

[3] R. Ramaswami, *Optical networks : a practical perspective*, 2nd ed. San Francisco, 2002.

[4] R. S. Ribeiro, "Simulação, Análise e Optimização de Sistemas FSK Ópticos," PhD, Electrónica e Telecomunicações, Universidade de Aveiro, Aveiro, 1994.

[5] G. Betts and W. Chang, "Crossing-channel waveguide electrooptic modulators," *Quantum Electronics, IEEE Journal of*, vol. 22, pp. 1027-1038, 1986.

[6] S. V. Hum, "Electro-optic Modulators for Radio-on-Fiber Applications," Master of Science, Electrical and Computer Engineering, Calgary, Calgary, 2001.

[7] M. Schwartz, *Information, transmission, modulation and noise*, 4th ed. New York, 1990.

[8] A. B. Carlson, *Communication systems : an introduction to signals and noise in electrical communication*, 4th ed. Boston (MA), 2002.

[9] S. Haykin, *Communication systems*, 4th ed. New York, 2001.

[10] "Using Error Vector Magnitude Measurements to Analyze and. Troubleshoot Vector-Modulated Signals," *Agilent Product Note PN. 89400-14*.

[11] I. Frigyes, "Radio over Fiber: Application, Basic Design and Impact on Resource Management," ed. Budapest University of Technology and Economics, 2005.

[12] D. Wake, *et al.*, "Radio over fiber for mobile communications," in *Microwave Photonics, 2004. MWP'04. 2004 IEEE International Topical Meeting on*, 2004, pp. 157-160.

[13] B. Kalantari-Sabet, *et al.*, "Performance Impairments in Single-Mode Radio-Over-Fiber Systems Due to MAC Constraints," *Lightwave Technology, Journal of*, vol. 26, pp. 2540-2548, 2008.

[14] A. M. J. Koonen, *et al.*, "Perspectives of Radio over Fiber Technologies," in *Optical Fiber communication/National Fiber Optic Engineers Conference, 2008. OFC/NFOEC 2008. Conference on*, 2008, pp. 1-3.

[15] H. Al-Raweshidy and S. Komaki, *Radio over fiber technologies for mobile communications networks*. Boston (MA), 2002.

[16] M. Sauer, *et al.*, "Radio Over Fiber for Picocellular Network Architectures," *Lightwave Technology, Journal of*, vol. 25, pp. 3301-3320, 2007.

[17] K. Hyo-Soon, *et al.*, "Low-Cost Multistandard Radio-Over-Fiber Downlinks Based on CMOS-Compatible Si Avalanche Photodetectors," *Photonics Technology Letters, IEEE*, vol. 21, pp. 462-464, 2009.

[18] L. Roselli, *et al.*, "Analog laser predistortion for multiservice radio-over-fiber systems," *Lightwave Technology, Journal of*, vol. 21, pp. 1211-1223, 2003.

[19] M. L. Yee, *et al.*, "Performance and Noise Analysis of VCSEL ROF Using Spherical-ended Multimode Fiber Coupling," in *ITS Telecommunications Proceedings, 2006 6th International Conference on*, 2006, pp. 503-506.

[20] H. B. Kim, "Radio over Fiber based Network Architecture," Elektrotechnik und Informatik, Technische Universität Berlin, Berlin, 2005.

[21] P. K. Tang, *et al.*, "Transmission of multiple wireless standards over a radio-over-fiber network," in *Microwave Symposium Digest, 2004 IEEE MTT-S International*, 2004, pp. 2051-2054 Vol.3.

[22] A. Ng'oma, "Radio-over-Fibre Technology for Broadband Wireless Communication Systems," Electrical Engineering, Eindhoven University of Technology, Eindhoven, 2005.
[23] W. Stallings, *Data and computer communications*, 5th ed. Upper Saddle River (NJ), 1997.
[24] G. P. Agrawal, *Fiber-optic communication systems*, 2nd ed ed. New York, 1997.
[25] Z. Xiupu, *et al.*, "A novel millimeter-wave-band radio-over-fiber system with dense wavelength-division multiplexing bus architecture," *Microwave Theory and Techniques, IEEE Transactions on*, vol. 54, pp. 929-937, 2006.
[26] X. N. Fernando and R. Yuen, "Analysis of Sub-Carrier Multiplexed Radio Over Fiber Link for the Simultaneous Support of WLAN and WCDMA Systems," *Kluwer Wireless Personal Communications*, 2005.
[27] M. T. Zhou, *et al.*, "Radio-over-Fiber Transmission of 1.25-Gigabit Ethernet Signal on 60-GHz Band Subcarrier with Performance Improvement and Wavelength Reuse," in *Communications, 2007. ICC '07. IEEE International Conference on*, 2007, pp. 2151-2155.
[28] L. Sang-Hoon, *et al.*, "Linearization of DFB laser diode by external light-injected cross-gain modulation for radio-over-fiber link," *Photonics Technology Letters, IEEE*, vol. 18, pp. 1545-1547, 2006.
[29] D. Wake, *et al.*, "An optically powered radio over fiber remote unit using wavelength division multiplexing," in *Microwave Photonics, 2008. Jointly held with the 2008 Asia-Pacific Microwave Photonics Conference. MWP/APMP 2008. International Topicsl Meeting on*, 2008, pp. 197-200.
[30] J. J. Vegas Olmos, *et al.*, "Dynamic Reconfigurable WDM 60-GHz Millimeter-Waveband Radio-Over-Fiber Access Network: Architectural Considerations and Experiment," *Lightwave Technology, Journal of*, vol. 25, pp. 3374-3380, 2007.
[31] I. P. Kaminow, *et al.*, *Optical Fiber Telecommunications: Components and Subsystems*: Academic Press, 2008.
[32] A. Ng'oma, "Design of A Radio-over-Fibre System For Wireless LANs," ed. Master of Technological Design Eindhoven University of Technology, 2002.
[33] E. I. Ackerman and C. H. Cox, "RF fiber-optic link performance," *Microwave Magazine, IEEE*, vol. 2, pp. 50-58, 2001.
[34] M. Movassaghi, *et al.*, "DFB laser RIN degradation in CATV lightwave transmission," in *Lasers and Electro-Optics Society Annual Meeting, 1998. LEOS '98. IEEE*, 1998, pp. 295-296 vol.2.
[35] C. Tae-Sik and K. Kiseon, "Effect of third-order intermodulation on radio-over-fiber systems by a dual-electrode Mach-Zehnder modulator with ODSB and OSSB signals," *Lightwave Technology, Journal of*, vol. 24, pp. 2052-2058, 2006.
[36] I. A. Kostko, *et al.*, "A radio-over-fiber link for OFDM transmission without RF amplification," in *Lasers and Electro-Optics Society, 2007. LEOS 2007. The 20th Annual Meeting of the IEEE*, 2007, pp. 339-340.
[37] A. Kaszubowska-Anandarajah, *et al.*, "Demonstration of Wavelength Packet Switched Radio-Over-Fiber System," *Photonics Technology Letters, IEEE*, vol. 19, pp. 200-202, 2007.
[38] Y. Le Guennec, *et al.*, "New optical microwave up-conversion solution in radio-over-fiber networks for 60-GHz wireless applications," *Lightwave Technology, Journal of*, vol. 24, pp. 1277-1282, 2006.

[39] C. W. Nelson, *et al.*, "Relative Intensity Noise Suppression for RF Photonic Links," *Photonics Technology Letters, IEEE,* vol. 20, pp. 1542-1544, 2008.
[40] H. L. Moura, *et al.*, "Power Estimation and EVM Evaluation of QAM Finite Sequences," *SEON's,* 2009.
[41] "https://mentor.ieee.org/802.15/dcn/08/15-08-0554-01-003c-comments-on-evm-and-required-study.pdf, at 14/12/2009," ed.
[42] C. H. Cox, *Analog optical links : theory and practice*. Cambridge, 2004.